THE UNIVERSITY OF GRONINGEN

MASTER THESIS

Sulphur chemistry in the inner regions of protoplanetary disks

Author:
Jelke Bethlehem

Supervisor:
prof. dr. I.E.E. (Inga) Kamp

A thesis submitted in fulfillment of the requirements for the degree of Master of Science

June 22, 2022

THE UNIVERSITY OF GRONINGEN

Abstract

Kapteyn Astronomical Institute
Faculty of Science and Engineering

Master of Science

Sulphur chemistry in the inner regions of protoplanetary disks

by Jelke Bethlehem

Sulphuric species in protoplanetary disks are still a mystery. The bulk of of the sulphuric abundance has not been observed and the gaseous compounds that have been observed only account for less than 1% of the cosmic abundance. For this project I am working with the Protoplanetary Disk Modelling code called ProDiMo. The aim of this thesis is to investigate in what form sulphur is present in the warm molecular layer of the inner 10 AU of a protoplanetary disc and make spectral predictions of SO2 to determine if this can be observed with JWST. The sulphur chemistry in the warm molecular layer of the inner 10 AU of a protoplanetary disc was determined to be primarily sulphur-oxygen chemistry. Based of spectral predictions with a resolving power of 3000, SO_2 is only observable for a disc with a carbon to oxygen ratio smaller than 0.7.

Contents

Chapter 1

Introduction to the Sulphur depletion problem

Sulphur is the 16th most abundant element on Earth, but why do we have sulphur on Earth? Planets form in protoplanetary discs (PPDs) around young stars. The chemical composition of a disc is defined by the molecular parent cloud and the chemical processes inside the disc. For discs most of the chemical composition is poorly constrained, especially for sulphur. Sulphur is an essential element for life as we know on Earth, it is part of several amino acids that are required for peptide synthesis (Semenov et al., 2018). Therefore sulphur is important for the origin of life and habitability of planets. In order to understand the abundance of sulphuric molecules for planets, we need a better understanding of the sulphur species in PPDs (Semenov et al., 2018).

Sulphur chemistry is not only poorly understood in discs, but also in other interstellar environments. In the diffuse interstellar medium (ISM) and in photon-dominated regions (PDRs) (Goicoechea et al., 2006) sulphur is observed to be close to the cosmic value. However in dense molecular gas the observed sulphur in the gas phase adds up to be only 0.1% of the cosmic abundance (Le Gal et al., 2019). In PPDs the gaseous molecules only add up to be less then 1% of the total sulphur reservoir (Kama et al., 2019). Most sulphur in PPDs is thought to be in refractory materials. Kama et al. (2019) estimated this by analyzing and fitting photospheric abundances, they found that $\approx 89 \pm 8\%$ of the cosmic sulphur abundance is locked in refractory materials.

The inner few AU of a disk, where the terrestrial planets form are heated by the star, therefore these will be hottest parts of the disc having temperatures ranging between a few thousand and hundred Kelvin. This hotter material is observable in the near infrared wavelength regime. The MIRI instrument on board of the James Webb Space Telescope (JWST) can observe between 5 and 28.5 microns (Wells et al., 2015). This wavelength range includes ro-vibrational lines of SO_2 (Bast et al., 2013) and H_2S. Therefore JWST can assess the sulphur budget inside 10 AU.

The two main goals for this thesis are as follows; first I will investigate in what form sulphur is present in the inner 10 AU of a protoplanetary disc. This will be done using ProDiMo (Woitke, P., Kamp, I., and Thi, W.-F., 2009). Secondly using this information and the models I will make predictions of SO_2 with the resolution of MIRI which is on board of JWST.

This thesis is structured as follows; chapter 2 will provide an overview of PPDs and sulphur. Chapter 3 will explain the disk modelling code ProDiMo. In chapter 4

I will first give some result providing information about ProDiMo, these are a comparison between ProDiMo and NAUTILUS (Ruaud, Wakelam, and Hersant, 2016). This to investigate the sulphur chemistry. Followed by the expansions made to the ProDiMo chemical network showing the sulphur chemistry. Finally in chapter 4 I will present SO_2 spectra and analyse how the SO_2 fluxes change with respect to the C/O ratio. Chapter 5 will conclude on the main sulphur bearing molecules in the inner disk and our detect ability to detect them. To wrap things up in chapter 6, I will discuss open questions and what could be improved in future works.

Chapter 2

Background theory

2.1 Protoplanetary discs

Protoplanetary discs are the byproduct of star formation and form out of a out of a rotating gas and dust cloud (Dominik, 2015). These rotating discs of dust and gas can extend for more than 100 AU and are found around almost all low mass stars (Williams and Cieza, 2011).

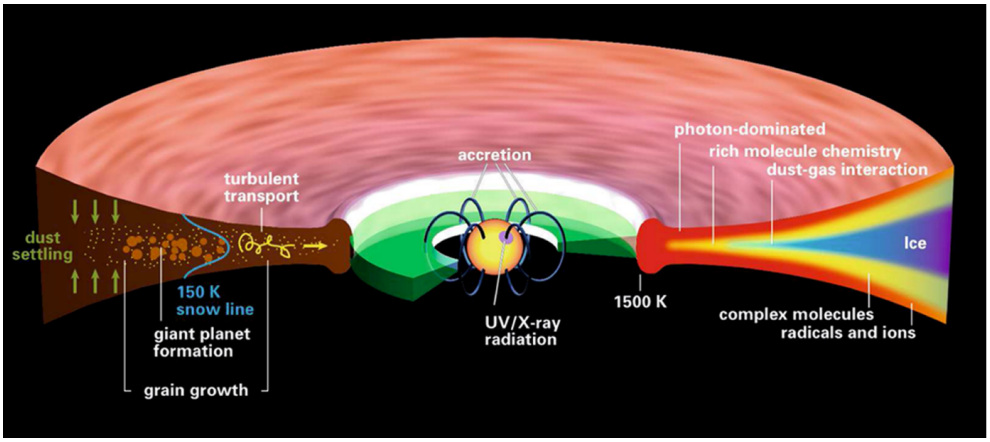

FIGURE 2.1: Illustration of the structure inside a protoplanetary disc around a sun like star (Henning and Semenov, 2013).

The disk can be split up in 3 different vertical layers (Henning and Semenov, 2013). On the right side in figure 2.1 these layers are illustrated with the colors red, yellow and blue. Seen from the top there is the layer indicated in red. This is the photon dominated layer which is a hot atomic layer with temperatures that can exceed 10000 Kelvin. The main heating mechanism are X-rays. This region is chemically very similar to photo-dissociation regions. It consists for the most part of ionized single atom species (Rab, 2017).

The next layer is the warm molecular layer. UV and X-ray photons get absorbed deeper into the disc. This causes the disk to be cooler which allows for the formation of simple molecules such as H_2, H_2O and CO. These molecules enable more efficient cooling mechanisms allowing the disc to become even colder which allows for the formation more molecular species. The temperatures in this layer vary between roughly 1000 and 100 Kelvin (Woitke, 2015a). This region is the region that I am most interested in for this thesis, especially the areas with a temperature around a few 100 Kelvin inside a radius of 10 AU.

The deepest part of the disc is given in blue, also known as the midplane which consists primarily of ices. This region starts around an optical extinction of 10. In

this layer the gas and dust temperature are about equal and temperatures are around 10 to 100 Kelvin (Woitke, 2015a). This is cold enough for most molecular species to freeze out on to the dust grains.

The left side in figure 2.1 illustrates the process of dust settling. This is due to the vertical component of gravity. Dust is very important for our understanding of protoplanetary discs. The dust mass accounts in general only for 1% of the total disc mass (Waters, 2015). Dust is important for determining the opacity of the disc and for surface chemistry. In most cases dust particles consist of silicates. Some common elements to find in dust particles are, O, Si and Mg (Waters, 2015). Furthermore dust grains will become the building blocks for planet formation, meaning their initial composition and distribution can be a determining factor for the type of planet that is formed. For my thesis the most important effect of dust is the role it plays in the chemistry. Dust grains are required for surface chemistry and ice formation.

Modelled objects in this thesis

There have been several methods and systems in the past that classified protoplanetary discs and related objects. Currently there is enough terminology to form a "diskionary" (Evans et al., 2009). For my research I have used information on two different types of objects, which are a standard disc around a TTauri star and a molecular cloud with the elemental properties of the Taurus Molecular Cloud TMC-1.

Molecular clouds are objects consisting of gas and dust with rather high densities ($\geq 10^4$ cm^{-3}), low temperatures between 10 and 100 Kelvin and sizes of 1-5 parsec (Maciel, 2013). If a dense part of a molecular cloud becomes gravitationally unstable and collapses with rotation it can form a star with protoplanetary disc (Dominik, 2015). Molecular clouds are the birthplace of Protoplanetary discs. TMC-1 is a dark cloud, which means it shows no signs of having star forming regions (Maciel, 2013). Eventually discs will form alongside young stellar objects (YSOs) from the densest parts inside a cloud such as TMC-1.

TTauri stars are young solar like stars, these stars are a couple of million years old. TTauri stars are similar in mass to our sun, therefore it can be expected that they evolve in the same way as our sun. The stars are very active and emit strong X-ray emission (Rab, 2017).

2.2 Sulphur

2.2.1 Elemental importance

Sulphur is element number 16 in the periodic table, in the same column as oxygen. Sulphur is chemically similar to oxygen therefore one could expect sulphur and oxygen to behave similar (Oppenheimer and Dalgarno, 1974). Oxygen is really important for us but the same could be said for sulphur.

Sulphur is considered to be essential for life. Sulphur bearing amino acids such as cysteine ($C_3H_7NO_2S$) and methiodine ($C_5H_{11}NO_2S$) are very important for peptide synthesis. Peptide synthesis is required for most living organisms (Semenov et al., 2018). Furthermore sulphur also plays an important role for our atmosphere. In the past sulphur could have been partly responsible for the formation of a snowball Earth (Macdonald and Wordsworth, 2017). The emission of sulphur into the stratosphere by volcanoes is known to cool the Earth for several years after the eruption. Besides cooling, atmospheric sulphur also increases the albedo. Nowadays there is not enough volcanic activity to have a drastic impact on our climate. Records of the

past show that there have been time periods with much more volcanic activity. In these times the sulphur in the stratosphere assisted in the positive feedback loop that resulted into a snowball Earth (Gupta, Marshall, and Ferreira, 2019).

2.2.2 Observations of sulphur bearing species in discs

Observations of sulphur bearing species in discs are very limited. Only 5 species have been detected so far: CS, SO, H2S, H2CS and SO2 of which the last 3 are quite recent discoveries (Le Gal et al., 2021). However adding all the observed gas species together only makes up for at most 1% of the total sulphur abundance we see in our solar system (Le Gal et al., 2021). This problem is not restricted to only protoplanetary discs, but also pertains to dense molecular clouds. This is called the "Sulphur depletion problem". Sulphur must be hidden in some form that we do not observe. This could be for example a refractory specie such as FeS or sulphur allotropes S_n (Le Gal et al., 2019).

2.2.3 Sulphur allotropes

Allotropes are molecules containing no variety in atoms. For example O2 and O3 are allotropes of oxygen. Sulphur is special because it has a very large number of stable allotropes, which also exist in nature. Orthorhombic-α and monoclinic-γ are two species composed of cyclo-S_8 that are stable and solid up to roughly 110°C (Theilig et al., 1982). Allotropes have been proposed as a possible solution to the sulphur depletion problem. Sulphur allotropes are not efficiently formed in the gas phase, but they can form efficiently through surface chemistry (Vidal et al., 2017). Sulphur allotropes are likely to be embedded in dust grains (Calmonte et al., 2016) and therefore hard to observe. Their existence in protoplanetary disks has never been confirmed. Calmonte et al. (2016) have confirmed the existence of S_3 and S_4 in the coma of comet 67P/Churyumov-Gerasimenko.

2.3 Chemistry in protoplanetary discs

Protoplanetary discs are characterized by strong vertical and radial temperature and density gradients. This together with vastly different radiation field strengths throughout the disc leads to a huge variety in chemical reaction types.

2.3.1 Chemical reaction types

The chemical processes can be split into two different categories, the gas phase chemistry and the surface chemistry. The key difference is that surface chemistry requires the presence of a dust grain.

Gas phase chemistry

Looking at the bonds between atoms in the gas phase chemistry, the reactions can be divided in 4 different categories, which are specified in table 2.1. From figure 2.1, the photon dominated layer is where destruction and ionization reactions happen the most. This layer has some formation of molecules through ion-molecule chemistry, however these formed molecules are dissociated immediately. The warm molecular layer is where most of the molecular gas phase chemistry occurs. Deeper in the disc

less radiation reaches through the vertical extinction. Thus higher up in the disc there is mainly ion chemistry, and deeper in the disc is more neutral chemistry. In the midplane almost no gas phase chemistry occurs as most species are frozen. In ProDiMo freezing out of species on dust grains and desorbing due to dust, photons or cosmic rays is considered gas phase chemistry. Only when ices interact with other species it is considered surface chemsitry.

Bond	Reaction type	Example	
Formation	Radioactive association	$O + SO$	$\rightarrow SO_2 + h\nu$
	Three body reactions	$O + SO + M$	$\rightarrow SO_2 + M$
	Associative detachment	$H^- + O$	$\rightarrow OH + e^-$
Destruction	Photo-dissociation	$CS + h\nu$	$\rightarrow S + C$
	Dissociation by cosmic rays or X-rays	$NS + CR$	$\rightarrow S + N$
	Dissociative recombination	$H_2S^+ + e^-$	$\rightarrow HS + H$
Rearranging	Neutral-neutral	$C + NS$	$\rightarrow CS + N$
	Ion-molecule	$C^+ + HS$	$\rightarrow CS^+ + H$
	Charge transfer	$C^+ + H_2S$	$\rightarrow H_2S^+ + C$
	Ionization by cosmic rays or X-rays	$OCS + CR$	$\rightarrow OCS^+ + e^-$

TABLE 2.1: Different chemical gas phase reaction types, example reactions taken from ProDiMo output, CR stands for cosmic ray and M implies a third mass is required

Surface chemistry

One percent of the mass within the ISM is confided to dust grains. Dust is mainly produced as a byproduct when a star is dying (Shaw, 2007). In discs dust particles have quite a large range in size. From the small micron sized grains all the way to planetesimals of 10000 km (Waters, 2015). In general dust particles have a silicate core which is enclosed by a mantle of refractory organic material (Shaw, 2007). On this outer layer ices created from volatile species can form. Chemistry involving ices in the outer layer of a dust grain is what we call surface chemistry. This concerns all chemistry where either a product or reactants ends up on the surface of the grain. In contrast to gas phase reactions, surface reactions are still very poorly understood especially the chemical mechanisms remain unclear (Shaw, 2007). For my work I used a surface chemistry module that is still under construction. The details of this ProDiMo module will follow in the modeling section. Surface chemistry mainly happens in the icy regions of a PPD, which is close to the cold midplane. surface chemistry is all about building more complex molecules within the ice mantles. In table 2.2, several different types of surface chemistry reactions are given. There are many different types of surface chemistry reactions.

2.3.2 Sulphur chemistry networks

Sulphur chemistry has been studied for quite some time now. However the Sulphur chemistry is less well known than carbon and oxygen chemistry. In addition many of the known reactions have only been measured at room temperature, which limits the accuracy of those rates over a large temperature range (Hobbs et al., 2021). In 1995 a chemical model of a photon-dominated region in a dense molecular cloud was presented by Sternberg and Dalgarno (1995). This model described the gas phase chemistry in a dense molecular cloud that was exposed to intense far-ultraviolet

Ice	Reaction type	Example	
Formation		H# + S	$\rightarrow$ HS#
		S# + S#	$\rightarrow S_2$#
Destruction		HS# + H	$\rightarrow H_2S$
	chemidesorption	C# + S#	$\rightarrow$ CS

TABLE 2.2: Different surface chemistry reactions, example reactions taken from ProDiMo output. A # indicates that a specie is frozen

radiation (Sternberg and Dalgarno, 1995). This model included sulphur and the reaction network is shown in figure 2.2.

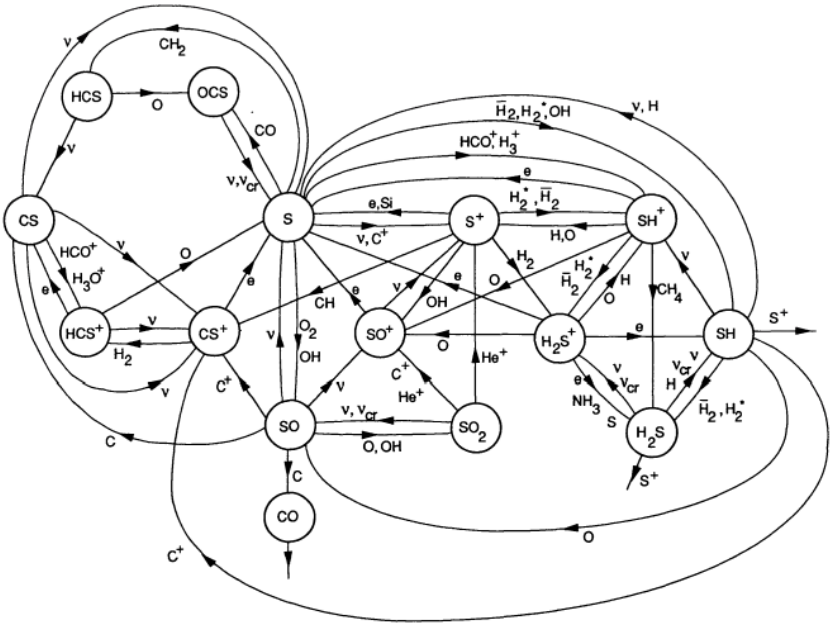

FIGURE 2.2: Gas phase sulphur network diagram from Sternberg and Dalgarno (1995).

The network contains 14 sulphuric species. Even though this is only a small network diagram it already shows several interesting and limiting formation pathways. For example the formation of SO_2. In this network diagram SO_2 can only be formed through SO. To compare this with newer networks, in UMIST2012 there are 9 formation pathways to create SO_2. From these 9 pathways 6 use sulphur species that are not present in this network diagram. Nowadays there are many models that include sulphur chemistry. The many different areas in a disc illustrated in figure 2.1, allow for a great range in temperature, densities and radiation fields. This requires a great amount of reactions for a complete network. Because of this vast amount of reactions it is impossible to make a clear full network diagram that gives an overview of the complete sulphur chemistry. On top of that every model has its own selection of reactions because many reactions involving sulphur do not have any experimental values and are based on assumptions and estimates (Moses, Zolotov, and Fegley,

2002). To deepen my understanding of the sulphur chemistry I created several network diagrams with the output of the ProDiMo code. However these networks have been simplified such that they are only valid for a specific temperature and density. Under these constraints it is possible to draw a diagram using only a part of the total reaction network. The networks are shown in chapter 4.

2.4 Mid infrared Spectra

Spectroscopy makes it possible to identify molecules in space. Knowing which species we have and their abundances gives us also information on the interactions of these species with their surroundings (Shaw, 2007). Molecules have 3 degrees of freedom; rotation, vibration and bending. These movements are transitions from one energy state to another and this transition results in the emission of photons. For the 3 degrees of freedom the resulting photon usually falls into the wavelength range from near-IR up to millimeter (Dionatos, 2015). The energy difference between the states determines the energy and therefore the wavelength of the photon. Molecules can also undergo electronic transition however these transitions have very high energies resulting in photons of optical or UV wavelength. Each molecule has its own spectral lines. All lines for a single species form the spectral profile which is similar to a finger print for that species. Observed spectral lines are broadened by different mechanisms.

There are 3 broadening mechanism. First there is the natural broadening, this is caused by the uncertainty principle (Kamp, 2015). If an excited state has a very short lifetime the uncertainty in energy is high. This effect has the smallest contribution on a line profile (Shaw, 2007). Next there is pressure broadening which is caused by collision between molecules in a gas. Collisions slightly change the energy levels and therefore the width of the transition. As third mechanism there is Doppler broadening also known as thermal broadening. The distance between observer and specie is almost never constant. The molecule moves either towards us or away from us and this causes a shift in wavelength. Molecules in a disc or cloud do not have perfectly similar velocities. Thus this spread in velocities causes different Doppler shifts and therefore broadens the line (Shaw, 2007). Turbulent broadening is a specific case of Doppler broadening caused by turbulent motions.

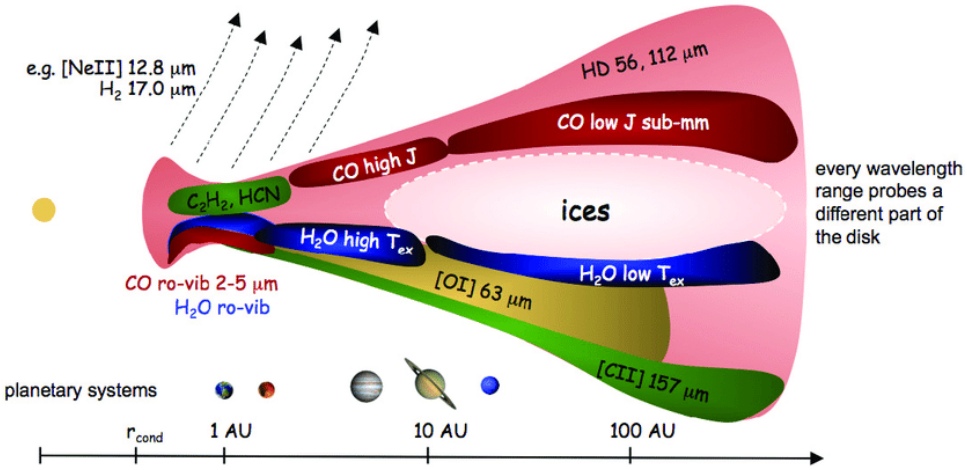

FIGURE 2.3: Illustration of line emitting regions inside a protoplanetary disk (Kamp, 2015)

In figure 2.3 the schematic of a flared disc illustrates which type of line emission to expect from specific parts of a disc. The line emission is dependent on excitation. Excitation is again controlled by the temperature which is why the regions are spread along different layers similar to figure 2.1. In general at large radii the wavelengths are between 100 micron and sub mm while the inner disc shows transitions at wavelength of a few to tens of micron. The figure shows that low rotational, high rotational and ro vibrational lines of H_2O and CO are spread over the full radius from low density areas in the outer disc to the dense hot inner part of the disc (Kamp, 2015).

2.4.1 Ro-vibrational lines of SO2

The energies required for vibration is larger than the one for rotation. Therefore it is unlikely to have pure vibrational transitions. Instead there is a rotation-vibration spectrum where both the rotational and vibrational states change (Rybicki and Lightman, 1985). This transition is also known as a ro-vibrational transition. For a symmetric top molecule such as SO2 there are 3 different vibrational modes, symmetric, antisymmetric and the scissoring band. The symmetric and antisymmetric band radiate in the 4-10 μm regime (Rothman et al., 2013) while the scissoring band is visible between 16 and 23 μm (Bast et al., 2013).

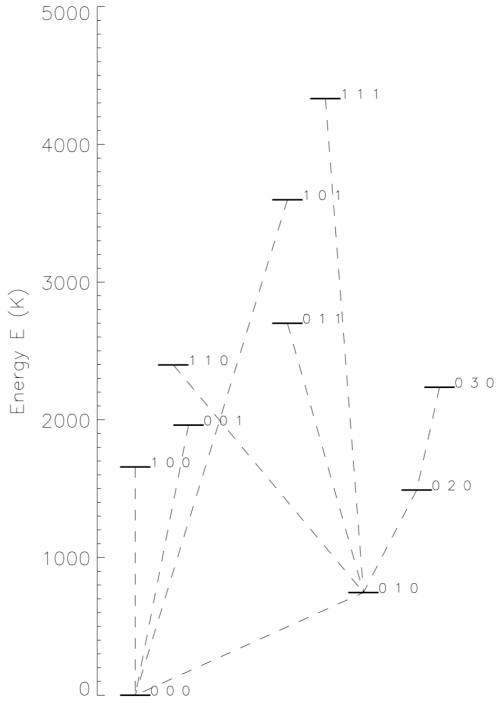

FIGURE 2.4: Energy levels of SO_2

Figure 2.4 shows all vibrational bands for SO_2. Notation for each band is given by (ν_1,ν_2,ν_3), Where ν_1 indicates the symmetric stretch active at 8.7 μm, ν_2 the scissoring band active at 19.3 μm and ν_3 the antisymmetric stretch active at 7.3μm. The original ProDiMo selection does not include the scissoring band. The code has been modified such that it takes both the original HITRAN selection chosen by Woitke et al. (2018) and the scissoring band introduced by Bast et al. (2013) for a total of 31968 lines. Each transition with the type source and amount of lines is given in table 2.3. The top two states from figure 2.4 are not taken into account.

Transition			Type	Amount of lines	Source
1 0 0	→	0 0 0	Symmetric	8291	Original ProDiMo selection
1 1 0	→	0 1 0	Symmetric	4043	Original ProDiMo selection
0 0 1	→	0 0 0	Antisymmetric	4904	Original ProDiMo selection
0 1 1	→	0 1 0	Antisymmetric	3557	Original ProDiMo selection
0 1 0	→	0 0 0	Scissoring	5914	Bast et al. (2013)
0 2 0	→	0 1 0	Scissoring	3727	Bast et al. (2013)
0 3 0	→	0 2 0	Scissoring	1532	Bast et al. (2013)

TABLE 2.3: SO_2 rovibrational transitions

2.4.2 MIRI instrument

The Mid-InfraRed Instrument (MIRI) (Rieke et al., 2015) is one of the instruments on board of JWST. MIRI is a camera and an integral field unit spectrograph that can observe near to mid infrared wavelengths from 5 to 28.5 μm. As stated in the previous section SO_2 has many rovibrational lines in this region. The high resolution is very important, a high resolution gives smaller wavelengths bins at which the flux

is blended. This allows to better untangle blended regions of observed fluxes with, for example SO_2 antisymmetric lines are blended with water lines at 7.3 μm. For MIRI the resolving power ($\lambda/\Delta\lambda$) is roughly 3000 for 5 μm and 1500 for 28.5 μm (Wells et al., 2015). Spitzer observed at similar wavelengths (10-37 μm) and has observed several sulphur species in PPDs such as CS, SO and H_2S with a resolving power of 600. JWST is significantly better as its predecessor, thus we hope to find better constrains and more sulphuric species.

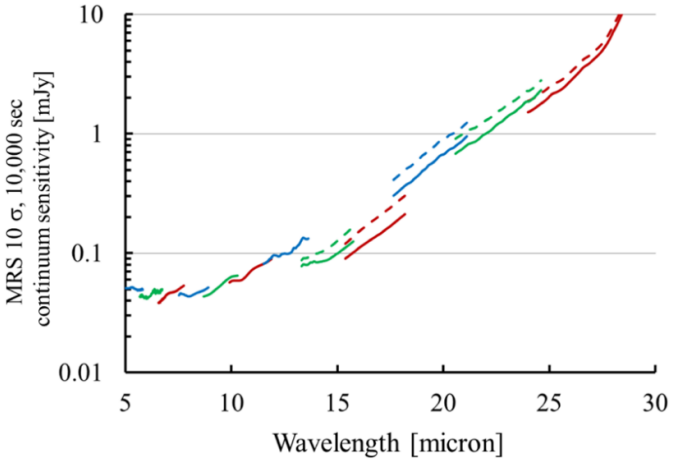

FIGURE 2.5: Sensitivity for MIRI, figure taken from Glasse et al. (2015). The dashed line indicates a high background case.

Figure 2.5 shows the expected sensitivity which relates directly to the minimum flux that can be observed. As the resolving power drops for higher wavelengths the sensitivity is better at low wavelengths. The figure shows the sensitivity after 10e4 seconds (about 3 hours) of exposure with a signal to noise ratio of 10.

Chapter 3

ProDiMo

In this chapter I shall describe the modelling code ProDiMo, which I used to analyze and research protoplanetary discs and the sulphur chemistry. ProDiMo is an acronym for Protoplanetary Disc Model (Woitke, P., Kamp, I., and Thi, W.-F., 2009) (Kamp et al., 2010) (Thi, Woitke, and Kamp, 2011) (Woitke et al., 2016) (Kamp et al., 2017).

3.1 Model structure

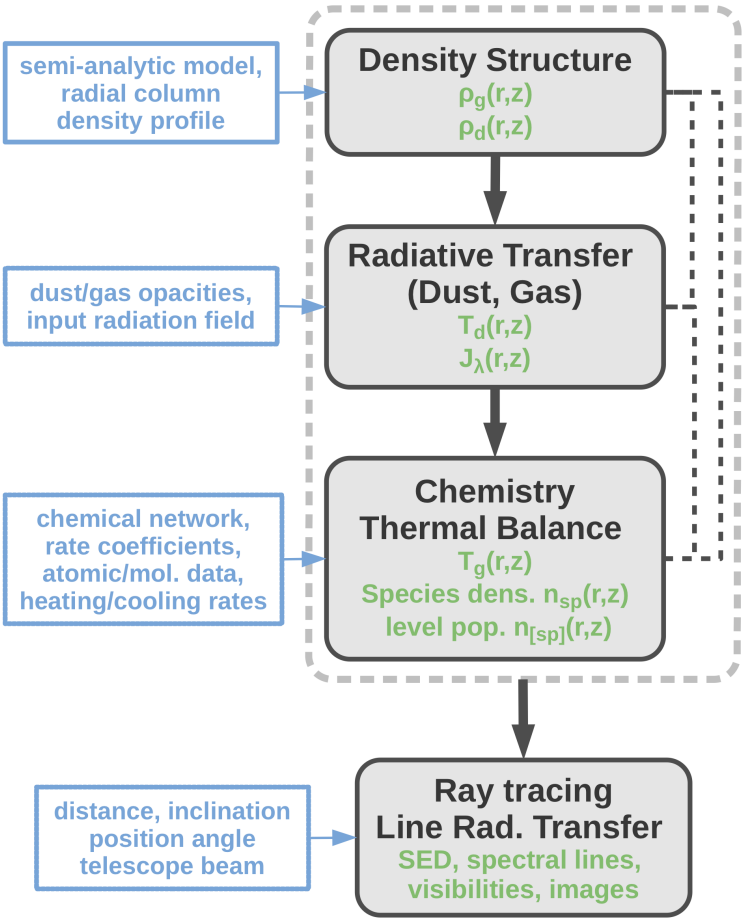

FIGURE 3.1: Flowchart showing the modeling approach used by ProDiMo (Rab, 2017)

In figure 3.1 the general code structure is defined. In blue all input parameters are defined, in black the specific step and in green the output per step. In the following subsections all processes in figure 3.1 will be discussed with their respective key equations.

3.1.1 Density structure

The first box in figure 3.1 determines the gas and dust distribution. The gas column density structure $\Sigma(r)$ is determined by a radial powerlaw with index ϵ with an exponential tapering off factor (Woitke et al., 2016)

$$\Sigma(r) \propto r^{-\epsilon} \exp\left(- \left(\frac{r}{R_{\text{tap}}}\right)^{2-\gamma} \right) \tag{3.1}$$

Where R_{tap} is the tapering off radius, ϵ the column density power index and γ the tapering off exponent. The tapering off exponent is standard assumed to be $\gamma = \epsilon$ (Woitke et al., 2016). Furthermore in the vertical direction the gas is assumed to have a Gaussian distribution:

$$\rho(r,z) \propto \exp\left(- \frac{z^2}{2H_g^2(r)} \right) \text{ [g cm}^{-3}\text{]} \tag{3.2}$$

$$H_g(r) = H_0 \left(\frac{r}{r_0}\right)^{\beta} \tag{3.3}$$

Here $\rho(r,z)$ it the gas mass density in cylindrical coordinates, H_0 is the reference gas scale height at radius r_0 and β is the flaring power index.

The model is set up with a fixed gas to dust mass ratio. Thus the gas distribution also gives the initial mass distribution for dust. For the dust grain size distribution a powerlaw is assumed:

$$f_0(a) \propto a^{-a_{\text{pow}}} \tag{3.4}$$

in which a is the particle radius, constrained between a given minimum and maximum. This distribution is assumed before dust settling is applied.

Dust settling changes the vertical dust distribution causing larger grains to be concentrated towards the midplane. The dust is affected by upward turbulent mixing and downward gravitational settling. This results in a distribution where the smaller grains remain higher up in the disc and the larger grains sink down to the midplane (Woitke, 2015b). Dust settling is implemented according to Dubrulle, Morfill, and Sterzik (1995).

3.1.2 Radiative transfer and line radiative transfer

After the structure has been set up there is a full continuum radiative transfer from X-rays to mm wavelength (Woitke, P., Kamp, I., and Thi, W.-F., 2009)(Rab et al., 2018). For the chemistry the radiation field needs to be known at each point in the disc. Therefore the radiative transfer equation is solved for every grid point and includes scattering and thermal emission. The radiation intensity is affected by extinction, absorption and scattering coefficients. The star is the main irradiation source but next to the stellar radiation there is also UV radiation because of accretion, coronal X-ray emmision and interstellar background radiation fields. The radiative transfer

equation is typically solved for 20 to 40 wavelength bands from 0.1 μm to mm range (Rab, 2017). This allows for a numerical approach of the radiative transfer equation in full 2D (Woitke, P., Kamp, I., and Thi, W.-F., 2009).

3.1.3 Heating and cooling balance of the gas

Determining the gas temperature of a disc is a very important step in the modeling. The gas temperature is directly linked to the density structure and therefore to the opacity and shape of the disc. Furthermore the temperature profile also determines the chemical composition and the strength of emission lines (Woitke, 2015a). The heating and cooling processes are therefore a fundamental component of modelling. The heating and cooling is strongly coupled to the chemical model.

To compute the gas heating and cooling balance in discs tens of thousands of lines need to be taken into account. Solving the line radiative transfer equation for every gridpoint would take way too much computational time. This requires solving the line radiative transfer equation 10^6 or even 10^8 times (Woitke, 2015a). For this problem ProDiMo uses a solution called the 'escape probability method'. The escape probability method calculates the probability if a photon escapes and is thus emitted. This can be either radially towards the star or vertical upward. This method does not allow for broad wavelength intervals as the opacity changes with wavelength. The full derivation can be found in the article by Woitke, P., Kamp, I., and Thi, W.-F. (2009).

This method is important as it determines the line fluxes that we may be able to observe. The escape probability method makes several assumptions that allow for analytic solutions to the line transfer equation (Woitke, 2015a).

To calculate the number density of a species n_i over time, the following rate equation (Rab, 2017) is solved;

$$\begin{aligned}\frac{dn_i}{dt} = &\sum_{J_F} k_j(T_g) n_l n_m + \sum_{J_F} k_j^{phot} n_l + ... \\ &- \sum_{J_D} k_j(T_g) n_l n_m + \sum_{J_D} k_j^{phot} n_l + ...\end{aligned} \tag{3.5}$$

The first row of equation 3.5 sums over all formation reactions for a species n_i, the rate equation for two body gas phase and photo reactions are shown however the dots indicate all remaining reactions. The second row indicates all destruction reactions, together they show the full formation or destruction of a single species. k indicates a rate coefficient and n_l and n_m give rate coefficients of which the units are dependent per type of reaction. These rate coefficients are often dependent on the gas temperature. Therefore to solve this equation the thermal balance is required. To calculate the temperature, the net gain of thermal kinetic energy is used. This is given by;

$$\frac{de}{dt} = \sum_k \Gamma_k(T_g, n_{sp}) - \sum_k \Lambda_k(T_g, n_{sp}) \tag{3.6}$$

where Γ_k indicates the heating rates and Λ_k the cooling rates in units of erg s^{-1} cm^{-3}, T_g is the gas temperature and n_{sp} indicates the species density. By assuming steady state, which means the formation and destruction of a species is equal thus the abundance is constant. This means net gain should be zero, thus for equation 3.5 $\frac{dn_i}{dt} = 0$. However the heating and cooling rates depend on T_g and the species densities n_{sp},

but the species densities also depend on T_g. This requires an iterative process where T_g is varied and the chemistry is solved many times until the parameters satisfy the equation (Woitke, P., Kamp, I., and Thi, W.-F., 2009). The steady state approach is computationally less expensive than solving the chemistry time-dependent. It can easily make a factor 10 to 100 difference in computing time (Rab, 2017). For this work I have used both types of chemistry, time dependent for molecular clouds and steady for PPDs.

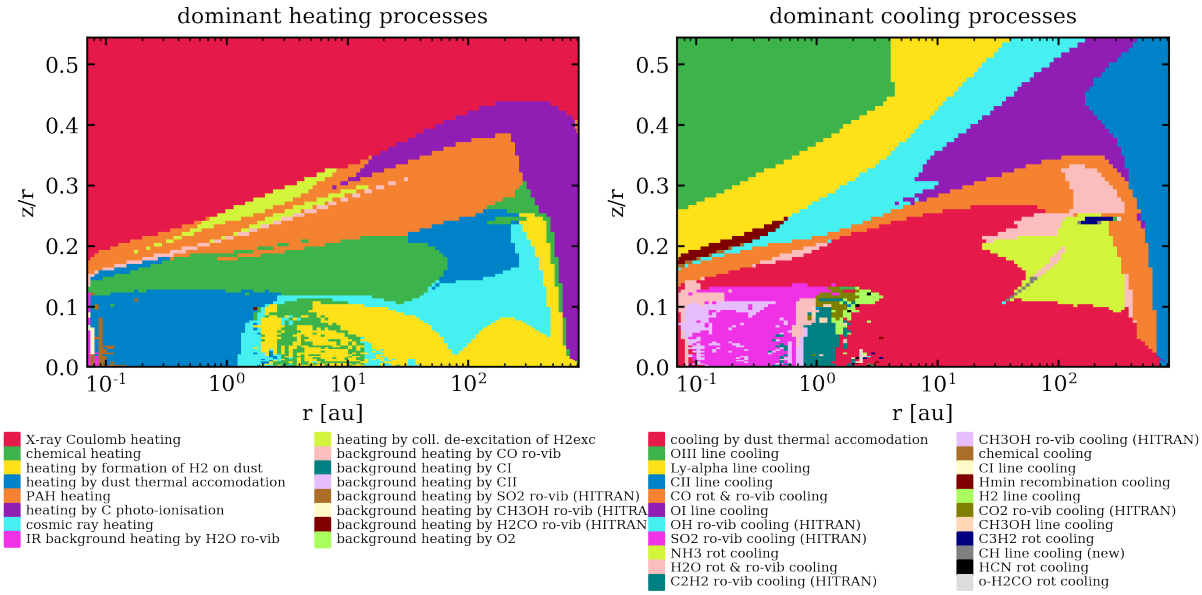

FIGURE 3.2: Dominating heating and cooling processes as function of position inside a disc

In figure 3.2 the most dominant heating and cooling processes are shown for each point inside the disc. This figure is generated for a standard TTauri disc model including rovibrational cooling lines. ProDiMo has more than 90 heating and 81 cooling processes(Rab et al., 2018). All these processes need to be taken into account to calculate the net gain of energy shown in equation 3.6. In layers where radiation cannot reach there is no heating and cooling through line emissions. The most important heating and cooling processes there are thermal accommodation on grains and formation of H_2 on dust. For accurate line cooling all abundances need to be known. From the abundances the fluxes are calculated through the escape probability formalism. It is assumed that the photons mainly escape through the vertical direction of the disc (Rab, 2017).

3.1.4 Molecular cloud approximation

ProDiMo can also model a molecular cloud by using a 0D mode. This means the model structure becomes much more simplified as it has a uniform density, temperature and dust grain distribution. The means processes such as the heating and cooling balance and radiative transfer get simplified. The chemistry is run time dependent in this model, but because of the simplifications through 0D these models have short computational times (few minutes). The molecular cloud models were used to compare the chemical network in ProDiMo with another chemical network used by NAUTILUS (Ruaud, Wakelam, and Hersant, 2016).

3.2 Chemistry module

The chemical and physical structure for ProDiMo are intertwined and cannot be calculated separate from each other. This section is to give some more details on how the chemistry works. In equation 3.5 the chemical rate coefficient k is introduced. Using this rate coefficient and the abundances of reactants, the chemical rate r can be calculated. The chemical rate r indicates how often a reaction occurs in $\mathrm{cm}^{-3}\,\mathrm{s}^{-1}$. Depending on the reaction type rates are calculated differently. For neutral-neutral chemistry the rate is calculated as follows:

$$r = k\, n_1\, n_2\, [\mathrm{cm}^3\,\mathrm{s}^{-1}] \tag{3.7}$$

where k is a value known as the reaction rate coefficient with units $\mathrm{cm}^3\,\mathrm{s}^{-1}$ for two body reactions. Every reaction has a rate coefficient that is either constant or temperature dependent. The reaction rate coefficient is calculated using reaction rate coefficients. For this thesis I took most reaction rate coefficients from the UMIST2012 database (McElroy et al., 2013).

The chemistry is written in a modular form so that it is possible to change the selection of species and reactions (Woitke, P., Kamp, I., and Thi, W.-F., 2009). For the reactions and rate coefficients the model takes 2 different inputs. First it uses the selection of species to pull all possible reactions from the UMIST2012 database (McElroy et al., 2013). On top of this database there is an additional input file that gets added to the rate coefficients from the UMIST database. This input file can be set to either only add reactions that do not exist in the UMIST2012 data or it can overwrite reaction rate coefficients extracted from UMIST. This modular approach allows for free control of the chemical network and respective rate coefficients. Aside this input there is one crucial reaction that is hard coded in ProDiMo. This is the H_2 formation on dust grains (Thi et al., 2018).

3.2.1 UMIST 2012 database

The UMIST2012 database works with different equations to calculate the rate coefficients dependent on the reaction type. In general the rate coefficient k is calculated with 3 parameters $[a, b, c]$. For two body reactions the rate coefficient follows from the Arrhenius law:

$$k = a\left(\frac{T}{300}\right)^b e^{-\frac{c}{T}} [\mathrm{cm}^3\,\mathrm{s}^{-1}] \tag{3.8}$$

For cosmic ray induced photo reactions this formula is

$$k = a\left(\frac{T}{300}\right)^b \frac{c}{1-\omega} [\mathrm{s}^{-1}] \tag{3.9}$$

where ω is the dust grain albedo (McElroy et al., 2013). For interstellar photo-reactions the rate coefficient is calculated as:

$$k = a e^{-cA_v}\ [\mathrm{s}^{-1}] \tag{3.10}$$

with the optical extinction A_v. Finally cosmic ray ionization and photo reactions are all calculated different not through a reaction rate coefficient. These rates are dependent on the photon and environment. The rate is given by

$$R^{ph} = \frac{1}{h} \int \sigma(\lambda) \lambda u_\lambda d\lambda \tag{3.11}$$

were h is the planck constant, σ is the photo cross section, λ the wavelength and u_λ the photon energy density.

These are several possible reaction types. ProDiMo has currently roughly 60 different reactions types build in. For most of them rates are calculated with one of the above given formulas. Furthermore UMIST is a gas-phase only database that does not include surface chemistry (McElroy et al., 2013). All reactions involving icy species have to be added on top of the database.

3.2.2 Sulphur in the standard DIANA network

The chemical in ProDiMo is also called the large DIANA network (Kamp et al., 2017), this network consist of 235 different species.The Sulphur chemistry in the large DIANA network consist of 11 different neutral species, 22 different ionized species and 11 ices. These species can be seen in table 3.1. Notable, is that none of the species in ProDiMo contains more than one S atom. UMIST contains 7 of these with several reactions and rates (H_2S_2, H_2S_2+, H_3S_2+, HS_2, HS_2+, S_2 and S_2+). In this thesis the sulphur allotropes S_2-S_8 are added to this network. Including ices and H_2# the total amount of species grows to 251.

CS	HCS	H_2CS	OCS	NS	SO
SO_2	S	HS	H_2S	SiS	
CS+	HCS+	H_2CS+	H_3CS+	OCS+	HOCS+
NS+	HNS+	SO+	SO_2+	HSO_2+	S+
S++	S+++	HS+	H_2S+	H_3S+	SiS+
HSiS+					
CS#	HCS#	H_2CS#	OCS#	NS#	SO#
SO_2#	S#	HS#	H_2S#	SiS#	

TABLE 3.1: All Sulphur bearing species present in the large DIANA chemical network with 235 species

3.2.3 Surface chemistry

Dust grains also play an important role in the chemical network. Species freezing out on dust grains create an icy mantle which can interact with the gas phase chemistry. Ice species are considered additional species for the chemistry (Woitke, P., Kamp, I., and Thi, W.-F., 2009). The cold surface chemistry can be split up in two different mechanisms. On one had we have the adsorption and desorbtion of species on to the grains and on the other hand there is the interaction between ice species on a grain and the gas phase or between two ice species on the grain. Adsorption and desorbtion is strictly speaking surface chemistry but in ProDiMo it is included as part of the gas phase chemistry.

Ice formation and evaporation

Simple ice formation on grains occurs by collisions. A gas species can adsorb to the surface of a grain if these two collide and the temperature is low. The adsorption rate

is determined by a sticking coefficient, the surface area of the grain and the thermal velocity of the gas phase species. By default a sticking coefficient of 1 is used (Woitke, P., Kamp, I., and Thi, W.-F., 2009). The stability of a frozen species depends on the adsorption energy. Desorption occurs if the internal energy of a species is greater than the adsorption energy.

Formation of species on dust grains

The rates for surface chemistry are calculated differently, surface chemistry does not use a rate coefficient but is dependent on the diffusion rates of both species on the surface. The rate for classical diffusion between two surface species i and j is given by;

$$R_{ij} = \kappa_{ij}(R_{diff,i} + R_{diff,j})N_i N_j n_d \tag{3.12}$$

where κ_{ij} is the probability for this reaction to occur, R_{diff} is the inverse of the diffusion time, N_i and N_j are the number of i and j on a grain and n_d is the dust-grain number density.

3.2.4 parameters and elemental abundance

Quantity	Symbol	Value
Stellar mass	$M_\star$	0.7 $M_\odot$
Stellar Luminosity	$L_\star$	1 $L_\odot$
Effective temperature	$T_\star$	4000 K
UV excess	f_{UV}	0.01
UV powerlaw index	P_{UV}	1.3
X-ray luminosity	L_X	10^30 erg s^{-1}
Interstellar UV	χ^{ISM}	1
Cosmic ray ionisation rate	ξ_{CR}	1.7e-17
Dust to gas mass ratio	δ	0.01
Disc mass	M_{disc}	0.01 $M_\odot$
Inner disc radius	R_{in}	0.07 AU
Tapering-off radius	R_{tap}	100 AU
Reference scale height	H_g(100AU)	10 AU
Flaring power index	β	1.15
Dust size	$a_{min} - a_{max}$	0.05 μm-3 mm
Dust mass density	ρ_{gr}	2.094 g cm^{-3}
Dust size dist. power index	a_{pow}	3.5
Turbulent mixing parameter	α_{settle}	0.01
Dust composition	$Mg_{0.7}Fe_{0.3}SiO_3$	60%
	amorph. carbon	15%
	Porosity	25%

TABLE 3.2: Parameters used for modeling a standard TTauri disc

Table 3.2 shows all input parameters used for the protoplanetary disc run. Table 3.3 has all of the input parameters required for a molecular cloud. A molecular cloud also uses the input files from a disc so therefore a lot of parameters are similar but

	Molecular Cloud
Number density	5e3 [cm-3]
Dust temperature	10 K
Gas temperature	10 K
Dust size	0.1 μm
Dust to gass mass ratio	0.01
Dust mass density ρ_{gr}	3 g cm^{-3}
Cloud extinction (A_v)	10
Interstellar UV field χ^{ISM}	5
Cosmic ray ionisation rate ξ_{CR}	1.3e-17
Time steps	48 end time = 1e6 years
	64 end time = 1e7 years

TABLE 3.3: Parameters used for modeling a molecular cloud with TMC-1 elemental abundance

Element	Standard TTauri disc	Molecular Cloud (TMC-1)
H	12.00	12.00
He	10.984	10.954
C	8.14	8.23
N	7.90	7.792
O	8.48	8.38
Ne	7.95	3.301
Na	3.36	3.845
Mg	4.03	3.903
Si	4.24	3.903
S	5.27	7.176
Ar	6.08	
Fe	3.24	3.477

TABLE 3.4: Elemental abundance in the models, abundances are given with respect to H in units of $log_{10}(n_X/n_H) + 12$

have different values. The number of timesteps are logarithmic spread between at time of 0 and the indicated end time. In table 3.4, the standard TTauri elemental abundance with depleted sulphur and TMC-1 elemental abundance is given. The solar value of sulphur is 2 orders of magnitude larger than the standard TTauri value (7.27).

Chapter 4

Results

The first goal of this thesis is to investigate in what form sulphur is present in the inner regions of protoplanetary discs. To achieve this, I compared the chemistry of the protoplanetary disc modeling code ProDiMo with the three-phase model NAUTILUS (Ruaud, Wakelam, and Hersant, 2016) for a molecular cloud model.

4.1 Molecular cloud comparison

The goal of the comparison between the protoplanetary disc modeling code ProDiMo and the three-phase model NAUTILUS (Ruaud, Wakelam, and Hersant, 2016) is to investigate the sulphur chemistry. To minimize effects not from the chemical network, all physical parameters were set to be the same for both models (see table 3.3). The initial elemental abundances were agreed to be that of TMC-1 (see table 3.4). In the following, I describe the 4 main differences in the chemical results.

The standard large DIANA chemistry in ProDiMo contains 40 different sulphuric species and the NAUTILUS model 169 sulphuric species. Comparing these models is interesting because the chemistry in the models is based on different databases. ProDiMo uses UMIST as main database while NAUTILUS uses KIDA as main database. For this comparison I received 3 different data sets containing all abundances for a fixed set of timesteps from the NAUTILUS model.

The first big difference between both models is the presence of PAH species. PAH species in ProDiMo cause the chemistry for molecular species to be sped up. This effect is because PAH^- is good at holding on to electrons. This causes the electron abundance in ProDiMo to temporarily drop by 2 to 3 orders of magnitude with respect to the NAUTILUS model. Having less free electrons allows for more efficient ion-neutral chemistry. PAH species therefore play an important role in the charge balance.

Secondly, H, H^+, H^-, H_2 H_2^+, H_3^+, He and He^+ abundances all evolve similar over time with the exception of H^+. For the first 1000 years, the H^+ abundance in ProDiMo is depleted by 2-3 orders of magnitude with respect to NAUTILUS. After investigating this, I found that the highest producing H^+ reaction in NAUTILUS was not part of ProDiMo (Le Gal and Navarro Almaida, private communication). This is the reaction $CH + C^+ \rightarrow C_2 + H^+$, for which NAUTILUS uses the rate coefficient from the KIDA database.

A third point is that ProDiMo and NAUTILUS have different sets of adsorption energies. This includes also the species S, CS, HC_2S and SO_2. It is notable, that with

the exception of SO_2 all energies in NAUTILUS are higher than the ones in ProDiMo.

The fourth and final difference between the models is a fundamental difference in the surface chemistry approach. NAUTILUS uses multiple ice phases; they differentiate between surface and bulk ices. The bulk ices are not able to interact with the gas phase. ProDiMo does not differentiate between these types of ice. The models were run until a maximum time of 1e7 years. At this time the abundance of bulk SO_2 ice in NAUTILUS is of the order 1e-38. Abundances so small are are neglectable as The lowest possible value is 1e-40. Surprisingly bulk ice starts to form very late, after 1e5 years. The abundance for bulk SO_2 ice is roughly 1e-38 and for surface SO_2 ice around 1e-8 at a time of 1e7 years. If these models are to be run until steady state or at least several orders of magnitude longer than 1e7 years, bulk ice species might play a big role in differentiating the models. Thus for the end time of 1e7 years the difference in surface chemistry is neglectable but at longer timescales bulk ices could form in high abundances.

To conclude, both models have similar abundance patterns as a function of time for sulphur. For both models, after 1e7 years the dominating species is always atomic sulphur. After that, both models showed high abundances for H_2S ice when including surface chemistry, and SO, SO_2 without including surface chemistry and ice formation.

Based on the above findings several changes were made to ProDiMo. These changes include turning on surface chemistry, adding the sulphur allotropes S_2 to S_8 with their ices and adding the reaction $CH + C^+ \rightarrow C_2 + H^+$.

4.2 Adding Sulphur allotropes to ProDiMo

Model	Surface chemistry	Sulphur allotropes	frozen disc structure	C/O	Sulphur	g/d	$M_{disc}(M_\odot)$
1				0.46	Depleted	100	0.01
2				0.46	Solar	100	0.01
3		✓	✓	0.46	Depleted	100	0.01
4			✓	0.46	Depleted	100	0.01
5	✓		✓	0.46	Depleted	100	0.01
6	✓	✓	✓	0.46	Depleted	100	0.01
7	✓	✓		0.46	Depleted	100	0.01
8	✓	✓		0.46	Solar	100	0.01
9				0.46	Depleted	1000	0.001
10-23				$0.3 - 1.3^*$	Depleted	1000	0.001
24-37	✓	✓		$0.3 - 1.3^*$	Depleted	1000	0.001
38-51	✓	✓		$0.3 - 1.3^*$	Solar	1000	0.001
* = [0.3, 0.46, 0.7, 0.9, 0.95, 0.98, 0.99, 1.0, 1.01, 1.02, 1.03, 1.05, 1.1, 1.3]							

TABLE 4.1: All ProDiMo disc models used for analysis

All results shown in the subsequent sections are from the 51 disc models[1] shown in table 4.1. All models include rovibrational lines for the following molecules; H_2O, C_2H_2, CH_4, CO_2, NH_3, HCN, H_2CO, CH_3OH, NO, SO_2, OH and H_2S. These lines were first added by Woitke et al. (2018) and originate from the HITRAN database. The selection for the rovibrational SO_2 lines has been changed such that it contains all lines between 0.6 and 30 micron including the scissoring band from Bast et al. (2013).

[1] ProDiMo Revision: bbd08171 2022/01/31

In the following section the effects of adding sulphur allotropes and surface chemistry are illustrated by showing the abundance of several molecular species in the disc. The results are presented using vertical cuts at radii 1, 5 and 10 AU. These vertical cuts show species abundance versus the total hydrogen column density. The total hydrogen column density is the intergrated volume density as a function of height. Thus the total hydrogen column density can be seen as height in the disc. The species have been selected such that they contain all sulphur through out the entire vertical cut of the disk.

Model 1,3,5 and 6 from table 4.1 will be compared in this section. Model 1 is the standard TTauri disc model only containing gas phase with no added species. For model 3 sulphur allotropes have been added, for model 5 surface chemistry has been added and for model 6 both sulphur allotropes and surface chemistry is included. For model 3,5 and 6 the disc structure is frozen such that the density, temperature structure and radiative transfer are always kept the same as the values of model 1. Freezing the disc structure makes sure all changes in output are because of the changes I made to the chemistry.

Gas-phase chemistry

Sulphur allotropes have been proposed as a possible solution to the sulphur depletion problem. Hobbs et al. (2021) validated a new network which also contained the sulphur species S_2 to S_8. I have added all reactions regarding sulphur allotropes from Hobbs et al. (2021) to the ProDiMo chemical network. The added gas phase reactions can be found in table A.1. Together with these reactions the reactions for adsorption and desorption were added. The adsorption energies for sulphur allotropes are approximated such that the energy scales linearly with the amount of sulphur atoms $E_{ads}(S_n)$ = 1100 x n (i.e. E_{ads} S_2 = 2200 and E_{ads} S_8 = 8800, Le Gal private communication)

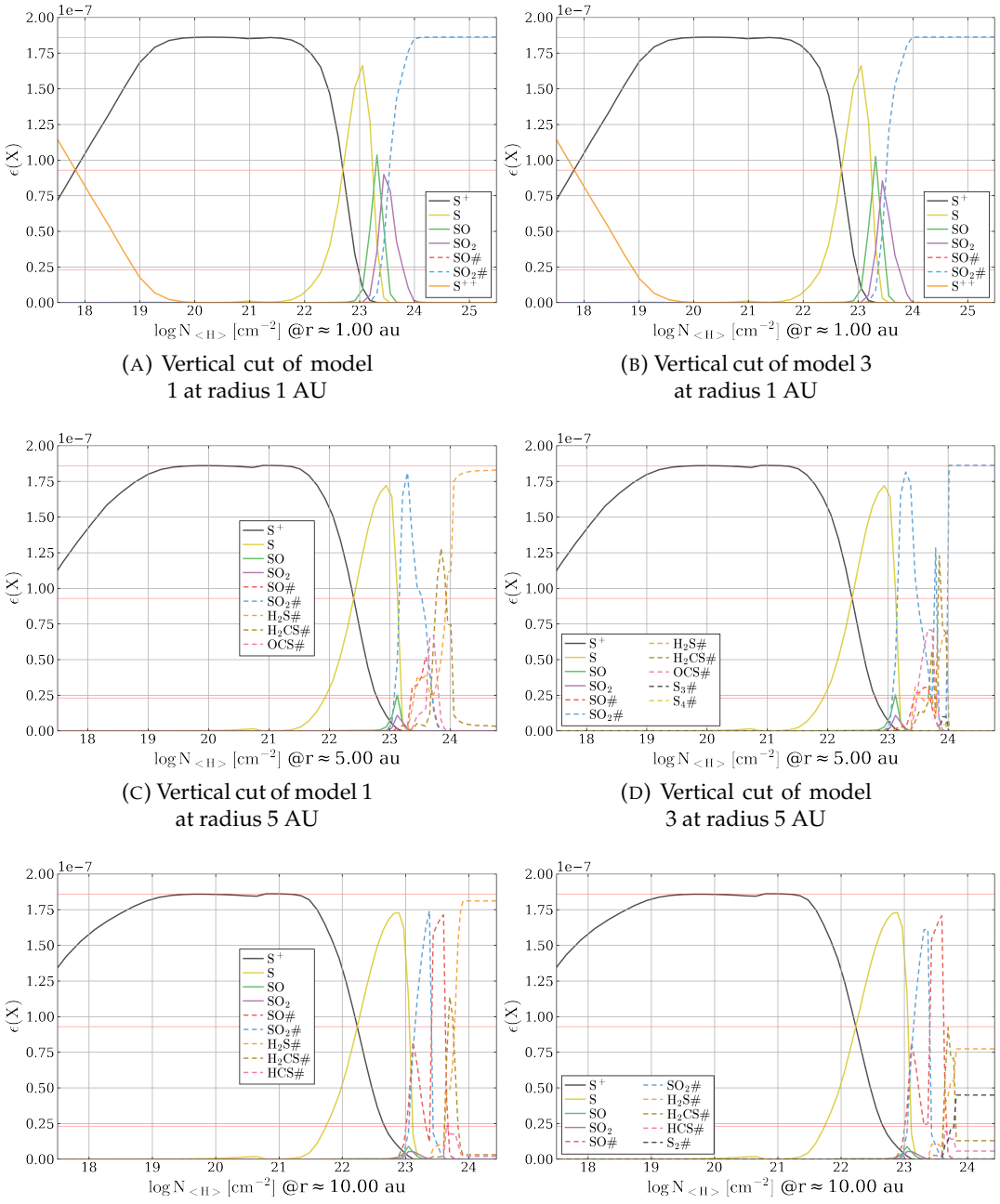

(A) Vertical cut of model 1 at radius 1 AU

(B) Vertical cut of model 3 at radius 1 AU

(C) Vertical cut of model 1 at radius 5 AU

(D) Vertical cut of model 3 at radius 5 AU

(E) Vertical cut of model 1 at radius 10 AU

(F) Vertical cut of model 3 at radius 10 AU

FIGURE 4.1: Vertical cuts of species abundance versus total hydrogen column density at radius 1, 5 and 10 AU of disc models 1 and 3 (from table 4.1). The horizontal red lines indicate 1, 1/2 and 1/8 times the elemental sulphur abundance

Figure 4.1 shows 6 vertical cuts of the disk, the standard TTauri model (model 1 DIANA gas phase chemistry) and model 3 which includes sulphur allotropes. Both models only include gas phase chemistry. The hydrogen column density is directly related to the physical height in the disc. At the disc surface all sulphur is in S^{++} which is only shown in the vertical cuts at 1 AU. In this subsection model 1 and model 3 from 4.1 will be compared at 3 different radii to analyze the effect of adding

sulphur allotropes to the gas phase chemistry. At 1 AU (panel A and B from figure 4.1), there is a decrease of roughly 0.1e-7 in gas phase SO_2 abundance at $\log N_H$ = 23.5 cm^{-2}, this difference is small enough to say that the abundances are unaffected by the changes made to the chemistry.
At 5 AU (panel C and D from figure 4.1) the gaseous species are similar, there is the same amount of S^+, S and SO_2 at the same hydrogen column densities. The ice species above column densities of $\log N_H = 23.7$ cm^{-2} change from H_2S# to first a mix of S_3# ,S_4# and H_2S# but above $\log N_H = 24$ cm^{-2} all sulphur is locked in SO_2#. Thus in the midplane there is a change in the most stable ice species from H_2S to SO_2 between model 1 and 3. This effect is caused by adding sulphur allotropes to the chemical network. In table A.1 it can be seen that sulphur allotropes only react with other sulphur allotropes and oxygen. The reaction between a sulphur allotrope and oxygen always gives formation of SO. This is a positive effect on the SO formation and therefore on the SO_2 formation. SO_2 has an adsorption energy of 5330 Kelvin and is therefore more stable as the sulphur allotropes S_3# (3300 Kelvin) and S_4# (4400 Kelvin) at these column densities.
Finally at 10 AU (panel E and F from figure 4.1), the vertical cuts of both models are the same up to a column density of $\log N_H$ = 23.7. I expected a similar situation as seen in the vertical at 5 AU (panel D figure 4.1). However instead of SO_2# the model has a mix of H_2S#, S_2# and H_2CS#. At this column density and radius the oxygen is depleted because it is frozen in OH# and H_2O#. At 5 AU, OH does not freeze. For these models the optical extinction of around 10 is reached at a column density of roughly $\log N_H$ = 23.7 cm^{-2}. Thus the warm molecular layer is not affected by the newly added reactions for sulphur allotropes.

Surface chemistry

Adding surface chemistry for the sulphur allotropes has quite a big impact on their formation rate. Vidal et al. (2017) stated that these species do not efficiently form in the gas phase at low temperatures. Instead they form through surface chemistry. I have added the surface chemistry reactions involving sulphur allotropes from Druard and Wakelam (2012). The added reactions are shown in table A.2. Only constructive reactions towards S_8# have been added. An increase in sulphur allotropes is expected in the disc where sulphur freezes out. The sulphur allotrope ices are extremely stable and with the reactions from table A.2 they have the option to react to S_8#. In panels D and F from figure 4.1, S_2#, S_3# and S_4# ices are appearing close to the midplane at column densities above $\log N_H$ = 23.7 cm^{-2}. Without surface chemistry the only way these species can react is by first desorbing into the gas phase. In the midplane this does not happen with high rates so therefore the sulphur is locked into sulphur allotrope ices that are not S_8#.

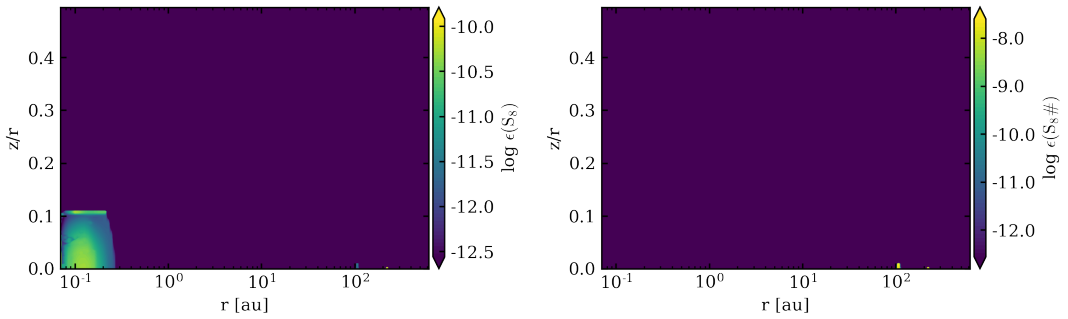

(A) Abundances S_8 and S_8# from model 3 (no surface chemistry)

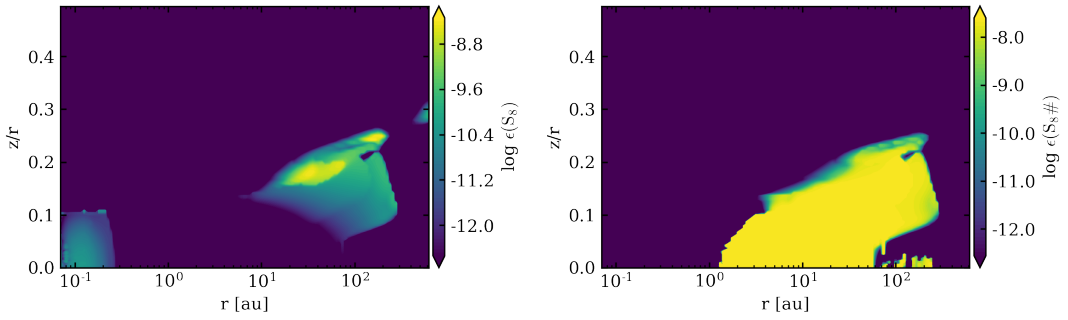

(B) Abundances S_8 and S_8# from model 6 (Including surface chemistry)

FIGURE 4.2: S_8 and S_8# abundances without (model 3) and including(model 6) surface chemistry, parameters of models can be found in table 4.1

Figure 4.2 shows that including surface chemistry leads to the full elemental abundance being in S_8# in the midplane. Because S_8# is formed through the ices the gas phase S_8 also increase because of desorbtion. This happen especially in top layer of the icy abundance in the outer disc. This is very clearly visible in the bottom left panel of figure 4.2. The inclusion of surface chemistry for sulphur allotropes influences therefore also the lower part of the warm molecular layer and might lock sulphur away in the S_8 allotrope causing a depletion in the gas phase.

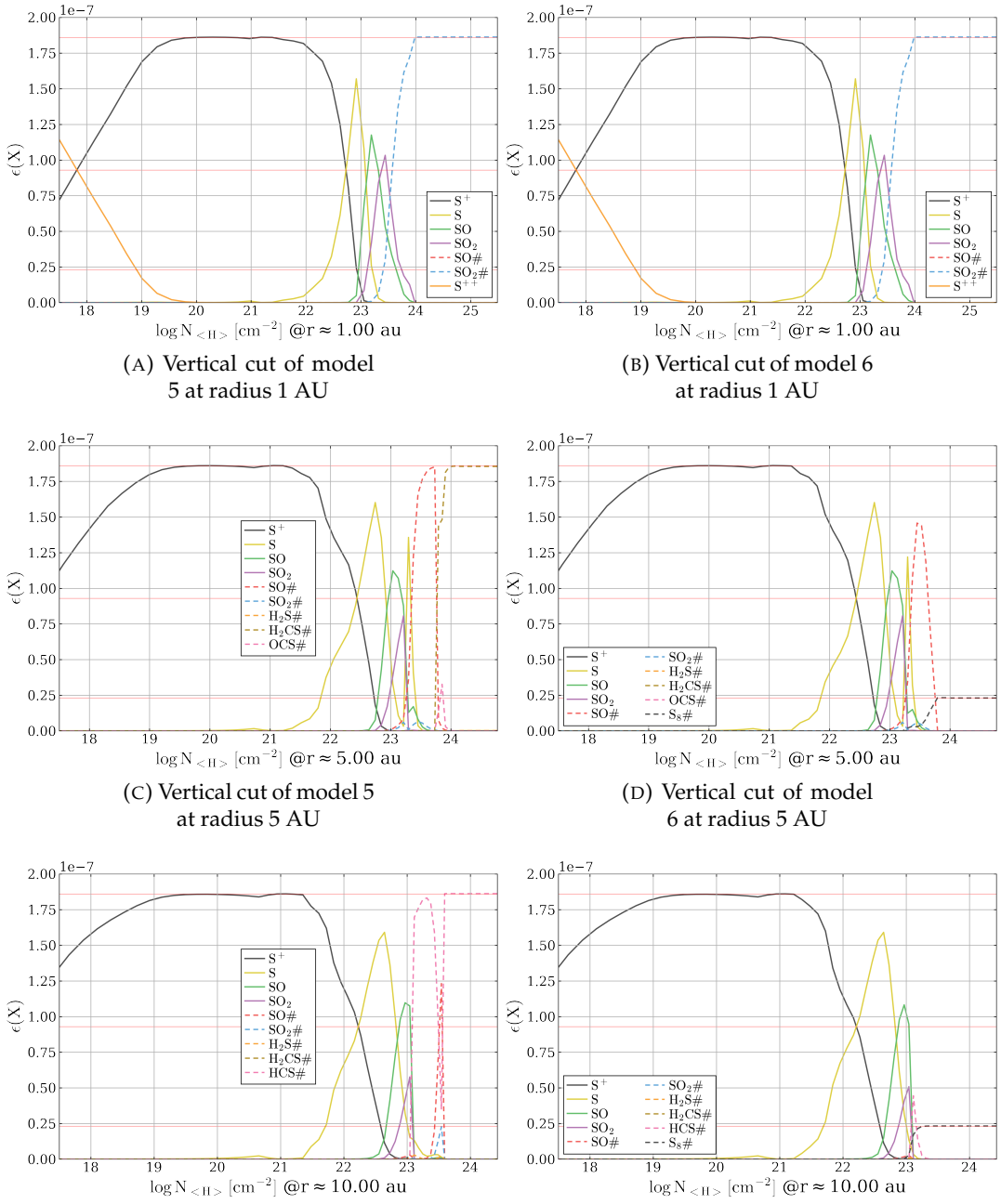

(A) Vertical cut of model 5 at radius 1 AU

(B) Vertical cut of model 6 at radius 1 AU

(C) Vertical cut of model 5 at radius 5 AU

(D) Vertical cut of model 6 at radius 5 AU

(E) Vertical cut of model 5 at radius 10 AU

(F) Vertical cut of model 6 at radius 10 AU

FIGURE 4.3: Vertical cuts of species abundance versus total hydrogen column density at radius 1, 5 and 10 AU of disc models 5 and 6 (from table 4.1). The horizontal red lines indicate 1, 1/2 and 1/8 times the elemental sulphur abundance

Model 5 and 6 (shown in figure 4.3) both include surface chemistry, the difference between these models is the presence of sulphur allotropes. Similar to model 1 and 3, for the radius of 1 AU the abundances do not change (panel A and B of figure 4.3. Neither the addition of allotropes nor inclusion of surface chemistry seem to have any effect on the sulphur abundances at a radius of 1 AU. For a radius of 5 (panel C and D) and 10 AU (panel E and F) the abundances change. In the midplane

all of the available sulphur freezes out in S_8#. The surface chemistry for sulphur allotropes is not complete with only the reactions shown in table A.2. At radius 5 AU the sulphur is completely frozen out in S_8# at column densities higher than $\log N_H$ = 23.8 cm^{-2} and for 10 AU at densities larger than $\log N_H$ = 23.2 cm^{-2} which also includes the bottom part of the warm molecular layer. Having a huge amount of sulphur from the warm molecular layer frozen in S_8# is not unlikely, as the sulphur depletion problem states that the majority of the sulphur abundance is depleted. To clarify the vertical cut images, the bottom red line indicates a abundance of 1/8 of the total sulphur reservoir. If the abundance of S_8 is equal to 1/8 of the total sulphur reservoir all sulphur is in S_8. The abundances are particle abundances with respect to [H] and not mass ratios.

To summarize, the addition of sulphur allotropes and surface chemistry changed the chemistry as expected. The sulphur-oxygen chemistry is enhanced such that the gas phase in the warm molecular layer is abundant with SO and SO_2 and the cold midplane is dominated by S_8#.

4.3 Sulphur chemistry in the inner disc

This section will show several network diagrams created based of the output from standard TTauri models with parameters given in table 3.2. This model includes both sulphur allotropes and surface chemistry. The network diagrams are made for very specific points in the disc model. At these points I analyzed the chemistry and only included reactions for which the rate was high. How high the minimum rate is is dependent on which grid point I examined. For radii 1 and 10 AU, I only chose the reactions that had rates within 5 orders of magnitude with respect to the highest rate. For the radius of 5 AU, the diagram includes reaction rates up to 7 orders of magnitude difference with respect to the highest reaction rate.

The diagrams are structured as follows: in the circles all sulphur bearing species with reactions that have high rates are given. Between the circles arrows indicate which way the reaction goes and the species on the arrow are the second reactants. The thickness of the arrow gives an indication of the rate. If multiple reactants are indicated, this means different reactions can occur. In this case of multiple reactions the thickness of the arrow gives the added sum of all reaction rates, where the first reactant has the highest contribution.

Diagram	Grid point (x,z)	r (AU)	z (AU)	T_{gas} (K)	T_{dust} (K)	A_V	n_H (cm^{-3})	Main S-specie
1	(22,25)	1.13	0.1526	120	120	3.1	7.4e11	SO_2
2	(80,37)	4.913	0.55	55	55	6.9	2.1e11	SO#
3	(90,44)	10.225	1.4826	46	45	1.6	2.5e10	S

TABLE 4.2: Specific conditions for the created network diagrams

In table 4.2 the radius, height, gas temperature, dust temperature, vertical optical extinction and density is given for each of the points for which the sulphur chemistry is analyzed using network diagrams. Each of these points were chosen such that they have a vertical optical extinction less than 10 ($A_V < 10$). This was done to ensure that the points are on the boundary between the warm molecular layer and midplane as shown in figure 2.1. This ensures that both active surface and gas phase chemistry

can be studied. Network 1 was created from a 60x60 grid size model, and model 2 and 3 from a 150x100 grid size model.

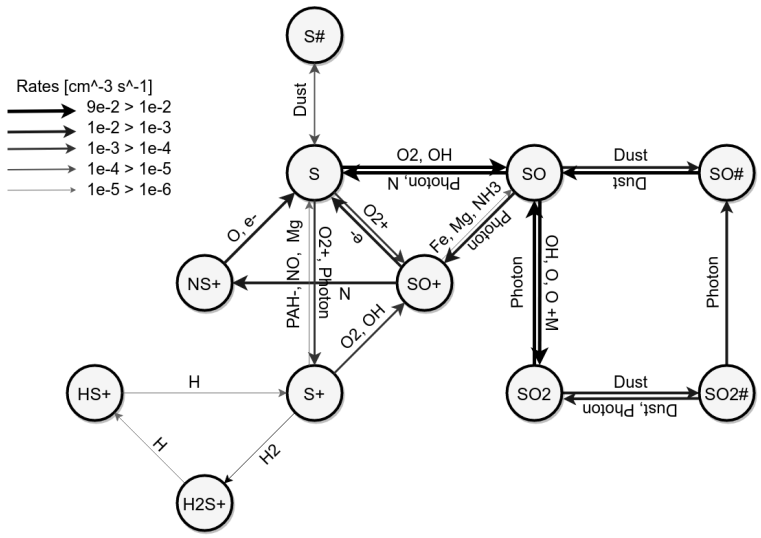

FIGURE 4.4: Sulphur network diagram 1 comprising only the highest reaction rates with a minimum rate of $1e-6$ [$\mathrm{cm}^{-3}\,\mathrm{s}^{-1}$]

Diagram 1 in figure 4.4 shows 11 sulphur species with their highest reaction rates. This network shows that at 1 AU we have mainly sulphur-oxygen chemistry, a single nitrogen reaction and a few very low rate hydrogen-sulphur reactions. Carbon never or very rarely interacts with sulphur under the conditions for this network shown in table 4.2. At this exact point in the disc, 99.8% of the total carbon abundance is locked in CO.

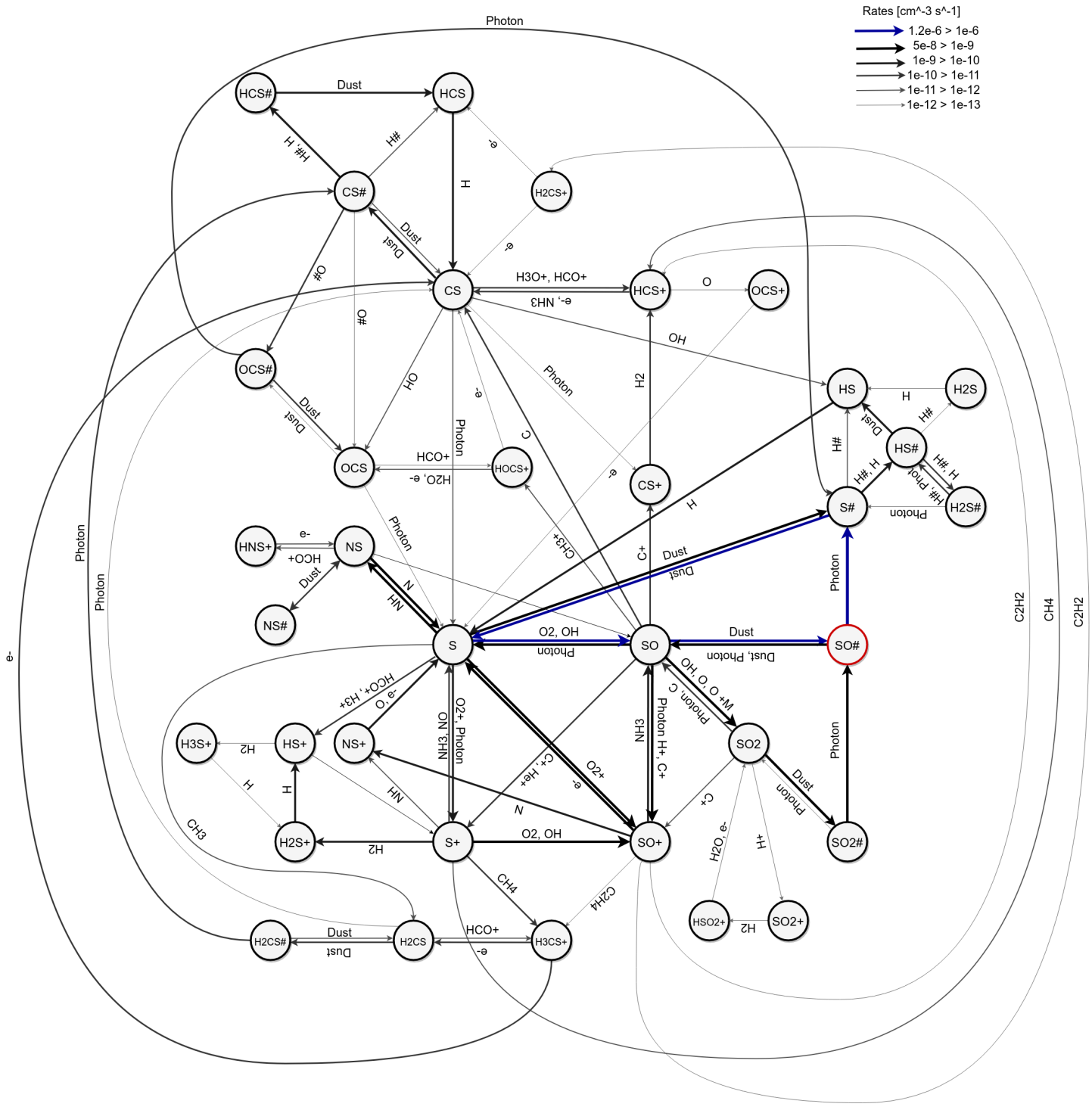

FIGURE 4.5: Sulphur network diagram 2 comprising only of the highest reaction rates with a minimum rate of 1e-13 [$cm^{-3}\,s^{-1}$]

At 5 AU the sulphur chemistry becomes more complex An interesting part is the hydrogen sulfide formation. Network 2 in figure 4.5 shows that at this point in the disc there are almost no active reactions forming H_2S, the reaction with the highest rate is the surface chemistry reaction $HS\# + H\# \rightarrow H_2S$. This means that either the formation pathways in the gas chemistry have extremely low rate coefficients for H_2S or that the reactants required have a very low abundance. In the chemical

network there are only 2 formation pathways for H_2S through neutral-neutral chemistry. These reactions are $HS + HS \rightarrow H_2S + H$ and $H_2 + HS \rightarrow H_2S + H$. Both of these reactions require HS as reactant. HS has many formation reactions but only a few of those are in figure 4.5. Most reaction rate coefficients for the formation of HS drop to zero for temperatures under 200K due to a strong temperature dependence.

Figure 4.5 shows that the main formation pathways for HS are through *S#*. This is either by forming *HS#* followed by desorption into HS or by direct hydrogenation into HS. This means that the main formation of HS is governed by surface processes. This finding is similar to the work by Semenov et al. (2018). They have a very similar conclusion for H_2S. Semenov et al. (2018) also has a very similar conclusion for the formation pathway of HS.

Figure 4.6 shows the sulphur chemistry at 10 AU. This network diagram is similar to the one at 1 AU (figure 4.4). The formation pathways for HS, go again through S#, which is directly related to H_2S. This is similar to network diagram 2 shown in figure 4.5.

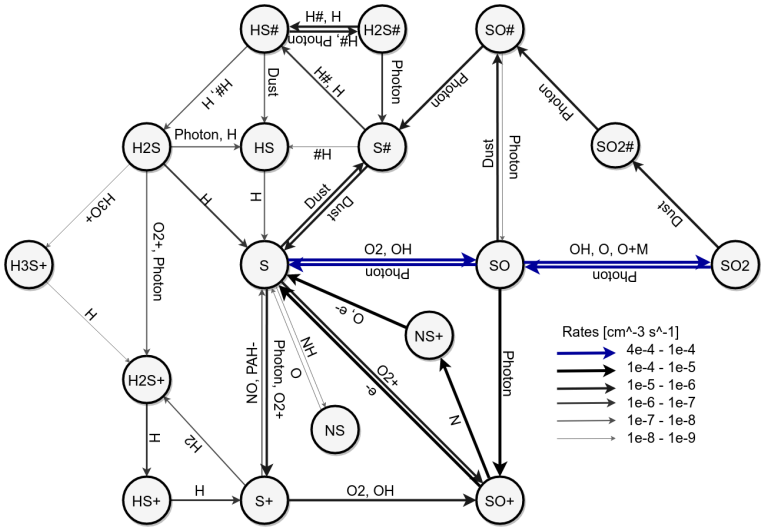

FIGURE 4.6: Sulphur network diagram 3 comprising only of the highest reaction rates with a minimum rate of $1e-9$ [$cm^{-3}\,s^{-1}$]

4.4 Fluxes as function of C/O ratio

As seen in the previous section, SO_2 is a main sulphur bearing molecule in the inner disc for the model including surface chemistry and sulphur allotropes (model 6 from table 4.1). SO_2 is very interesting from the observational perspective as it has many ro-vibrational lines. For the inner region depletion of oxygen is not an impossible scenario. There have been many observations of CS and non-detections of SO and SO_2, this suggests that many systems have a warm molecular layer with a high C/O ratio(Booth et al., 2021). Woitke et al. (2018) changed the carbon to oxygen ratio to bring the modeled fluxes closer to Spitzer/IRS observations. These observations show high HCN and C_2H_2 fluxes and low CO_2 fluxes. This could indicate a high C/O ratio.

Having more oxygen than carbon is a requirement to have SO2 abundant in the gas phase. The standard TTauri disc model has a carbon to oxygen ratio C/O = 0.46,

which is similar to the solar C/O ≈ 0.55 (Asplund et al., 2009), so there is roughly twice as much oxygen available as there is carbon. Figure 4.7 illustrates how the carbon and oxygen abundances are spread over various species in a vertical cut at a radius of 5 AU. The warm molecular layer defined by a column density of roughly 21 cm^{-2} < log $N_{<H>}$ < 23.5 cm^{-2}. Over this entire range all carbon is in CO. The chemistry in this region is oxygen based and not carbon based. If observed systems have a high C/O ratio this indicates that oxygen is locked in some specie, or carbon is more abundant with respect to oxygen. In the midplane the carbon is spread over two species containing multiple carbon atoms, together they contain approximately all carbon. The top horizontal line indicates the maximum oxygen abundance and the horizontal line at 1.38e-4 the maximum carbon abundance.

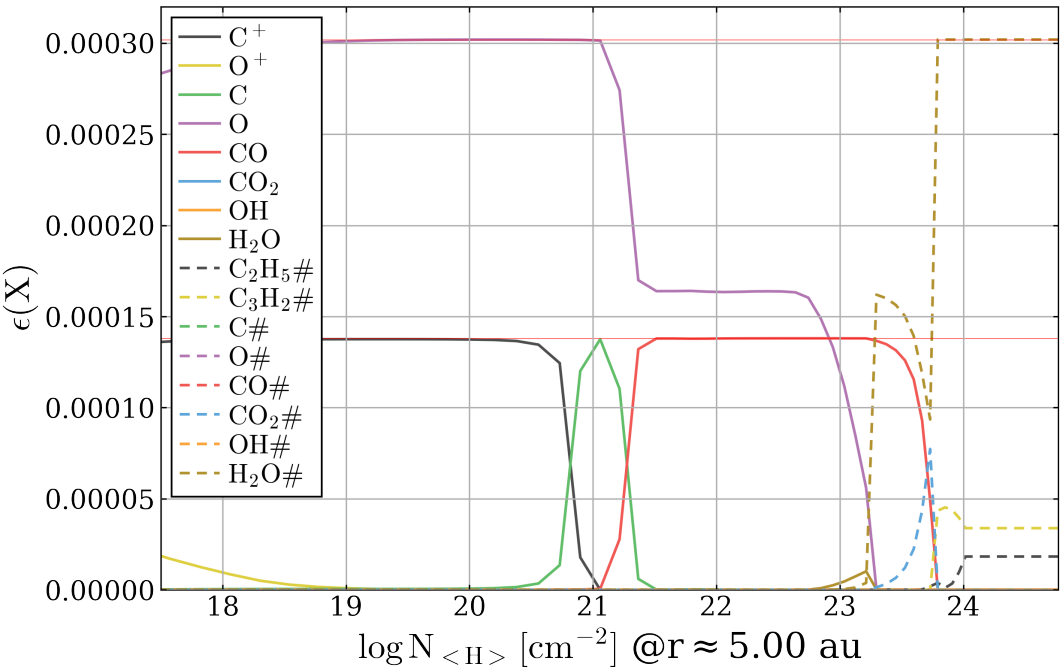

FIGURE 4.7: Vertical cuts of species abundance versus total hydrogen column density at radius 5 AU of disc model 6 (Model including surface chemistry and sulphur allotropes). The horizontal red line indicates the maximum elemental carbon abundance and the blue line the maximum oxygen abundance.

In table 4.1, 3 different series of 14 models each are given. The first series is created to reproduce the results from Woitke et al. (2018) for different C/O ratios. Woitke et al. (2018) did not include sulphur bearing molecules in his analysis. I now include SO_2 and H_2S ro-vibrational lines. I change the g/d ratio and disc mass (see table 4.1) to reflect the same values as used by Woitke et al. (2018). A higher g/d ratio has to be used to reach with the model flux values that are comparable to observed Spitzer observations.

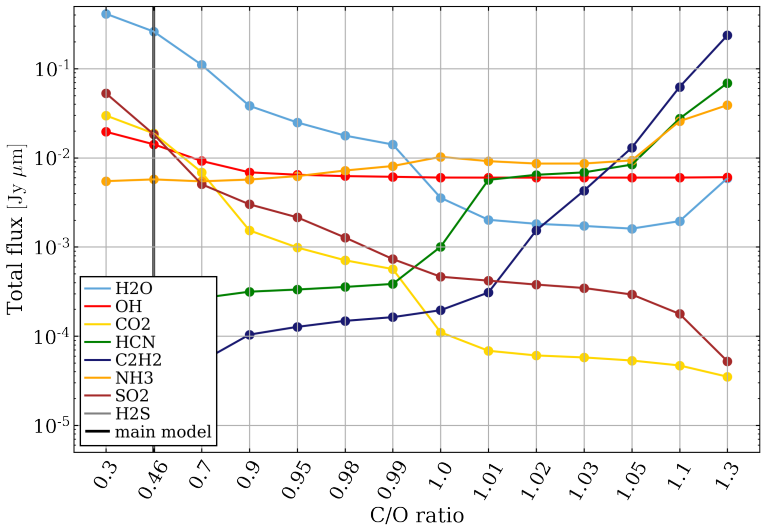

(A) Model series 10-23, no surface chemistry and no sulphur allotropes

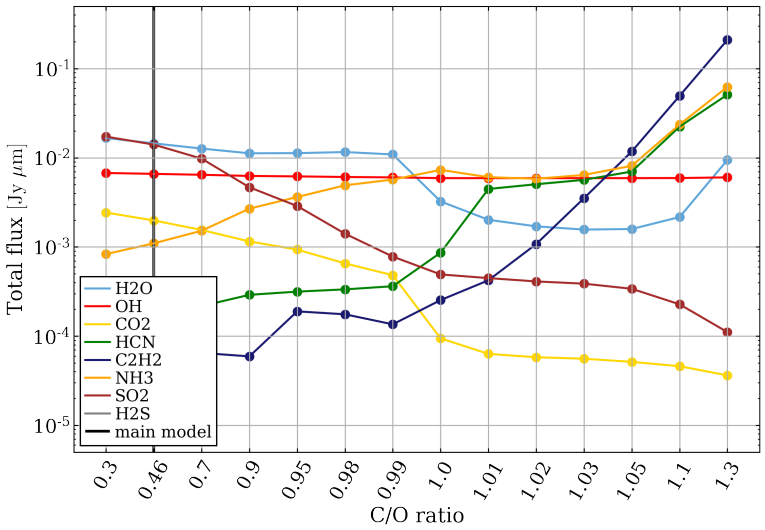

(B) Model series 24-37, include surface chemistry and sulphur allotropes

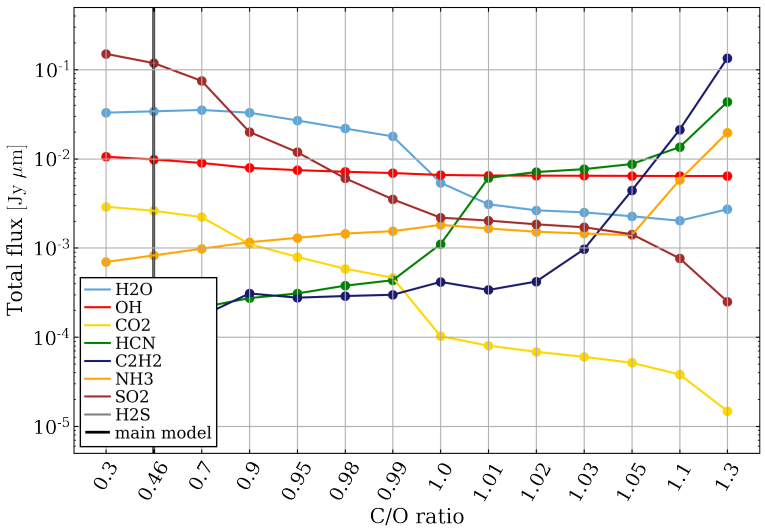

(C) Model series 38-51, include surface chemistry and sulphur allotropes and enhanced sulphur abundance

FIGURE 4.8: Total mid-IR line fluxes for 3 series of models, 10-23, models 24-37 and models 38-51 from table 4.1

Figure 4.8 shows 3 series of 14 models where for each model the flux for several species has been intergrated over the wavelength range of 5-28.6 μm. For each series this was done for 14 different C/O ratios to illustrate the effect the C/O ratio has on the SO_2 fluxes. This was done for 3 different series, for which the parameters can be found in table 4.1. For the third series the sulphur abundance is increased with 2 orders of magnitude with respect to the second series. 2 orders of magnitude increases in sulphur to the solar value. The wavelength range for which all fluxes have been intergrated corresponds to what the MIRI instrument on board of JWST will observe. A modest increase of C/O brings the model closer to Spitzer observations, which have fluxes around 10 to 100 mJy (Woitke et al., 2018).

Panel A from figure 4.8 is created to reproduce the results by Woitke et al. (2018). This reproduction was done to check if it possible to reach the correct flux values and validate the model.

In panel B from figure 4.8, surface chemistry and sulphur allotropes have been added to the model. Surface chemistry removes part of the flux for low C/O ratios, especially the fluxes for water lines drop because of this.

In the final series of models 38-51(panel C from figure 4.8) from table 4.1, the sulphur abundance is increased with 2 orders of magnitude to be equal to the solar value. The total SO_2 flux increases by roughly 1 order of magnitude for a low C/O ratio and half of that for a high C/O ratio. This increase of SO_2 flux at high C/O ratio is unexpected, because at high C/O ratio's (C/O > 1) sulphur is not the limiting element to form SO_2 but oxygen is. Therefore adding more sulphur should increase the SO_2 flux.

If observations indicate strong C_2H_2 or HCN fluxes this could indicate a depletion of oxygen. Thus there will probably be no SO_2 lines observed.

In all panels of figure 4.8, H_2S shows in the legend. The fluxes for H_2S are all of the order of 10^{-7} [Jy μm]. The fluxes for H_2S show no pattern with increasing C/O ratio.

4.4.1 Line emitting regions in the disc

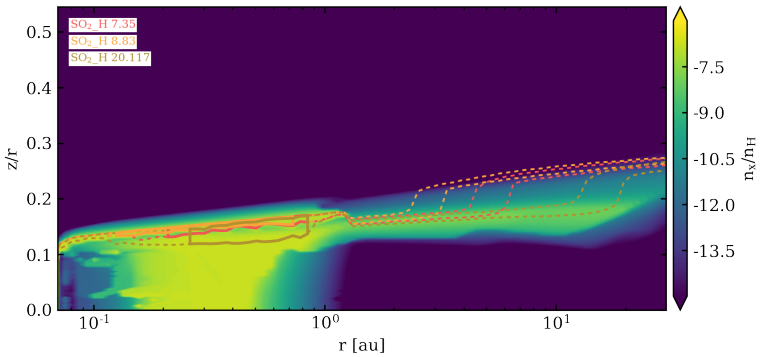

FIGURE 4.9: Emitting region for individual representative lines from the antisymmetric, symmetric and scissoring bands of SO_2 for model 10 from table 4.1, which has a C/O ratio of 0.3. The region within the countour lines is responsible for 50% percent of the flux. The background shows the sulphur abundance with respect to hydrogen.

In figure 4.9 the emitting region for representative lines from the antisymmetric, symmetric and scissoring band is shown. The flux intensity for the different rovibrational lines does not scale linearly with the change in C/O ratios. For all 3 models series the fluxes from the scissoring band decrease the least compared to the symmetric and antisymmetric band. This is to be expected as the lines from the scissoring band are emitted from deeper in the disc. Figure 4.9 illustrates that both the symmetric and antisymmetric lines emit from the top layer of the SO2 abundance while the scissoring band emits also from deeper in the disc. This is probably because the scissoring lines are more optically thin and can therefore emit from deeper in the disc. When the C/O ratio increases, SO_2 formation gets pushed deeper into the disc, meaning the vertical region for symmetric and antisymmetric lines shrink more than the region for the scissoring band.

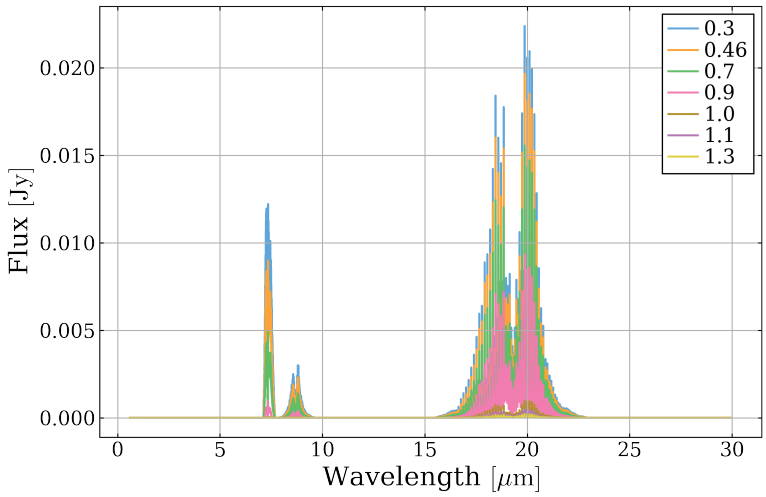

FIGURE 4.10: SO_2 spectra for various C/O ratios, models 24,25,26,27,31,36 and 37 from table 4.1

The effect that vertical region for symmetric and antisymmetric lines is more affected by the C/O ratio than the scissoring lines is visible in figure 4.10. In this figure it the flux for the symmetric band ($\approx$ 8.7 μm) and antisymmetric band ($\approx$ 7.3 μm) are decreasing significantly more with respect to the scissoring band ($\approx$ 19.3 μm). If SO_2 could be observed in a system with 0.7 < C/O < 1, there is a very high chance the scissoring band is observed.

4.5 Predictions for MIRI

4.5.1 Spectra

In the previous section the SO_2 fluxes are shown to be dependent on the C/O ratio. Assuming the observed disc has a C/O ratio of 0.46. Including the depleted sulphur abundance the ro-vibrational lines of SO_2 should be detectable, especially the fluxes from the scissoring band between 16 and 23 μm. Figure 2.5 shows that for an exposure of 10000 seconds, fluxes of 1mJy should be detectable for 20μm. The flux for the scissoring band in figure 4.11 is almost 20mJy at 20μm. Meaning there is a factor 20 excess for this model. The antisymmetric band will be hard to observe for this specific model. The sensitivity of MIRI is higher for this wavelength however the

blending with water lines can make this hard to observe. The sensitivity of MIRI is roughly 0.1mJy for 7-8 μm with an exposure time of 10000 seconds. The water fluxes did drop quite a bit with the addition of surface chemistry so in the case the water fluxes are one order of magnitude higher, the SO_2 fluxes for 7-8 μm are hidden in the water flux.

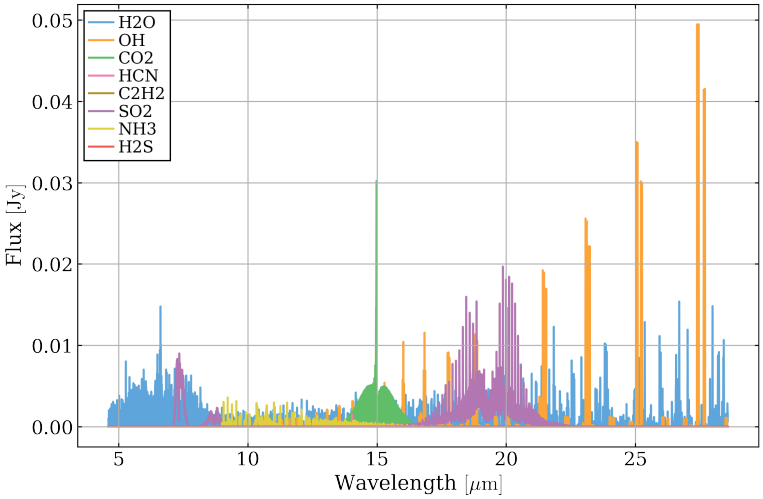

FIGURE 4.11: Spectra of sveral species for model 25 from table 4.1 with C/O=0.46

For model 26 which has C/O = 0.7 the fluxes from the scissoring band are still clearly stronger than the other lines. For this C/O ratio the fluxes from the antisymmetric and symmetric bands are lost within the water lines.

For the final model series that of which the sulphur abundance was increased to solar value. For the standard model with C/O=0.46 the SO_2 fluxes are around 70mJy for both the antisymmetric band and the scissoring band and 30mJy for the symmetric band. Meaning for this model all bands should be visible. The scissoring band should be observable even for C/O=0.9 But if the fluxes are so prominent they should have been detected already.

For the series of models (10-23) to reproduce Woitke et al. (2018) his work (panel A figure 4.8). The intergrated water fluxes are more than one order of magnitude larger than the intergrated SO_2 fluxes. Figure 4.12 shows that the water fluxes are dominating the SO_2 fluxes. This is even the case for a C/O ratio of 0.3.

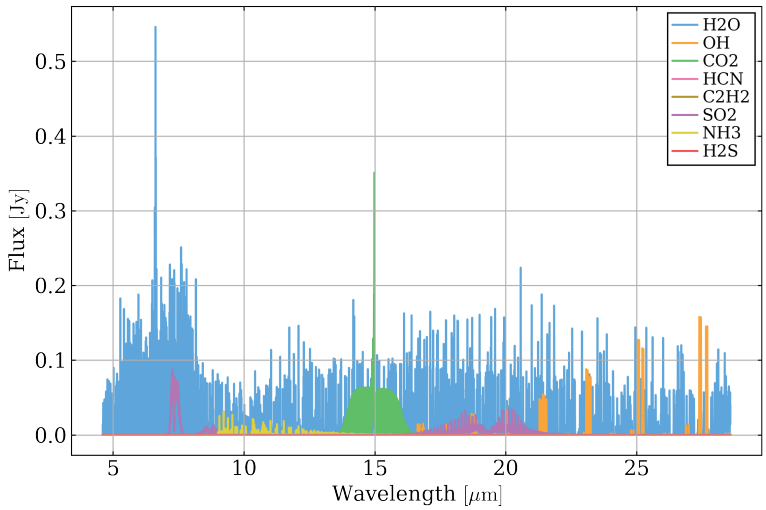

FIGURE 4.12: Spectra of several species for model 10 (no surface chemistry and no allotropes) from table 4.1 with C/O=0.3

3 hours is a long observing time. Normal observing times are somewhere between 0.5 to 1 hour. Assuming the sensitivity increases with $\sqrt{2}$ for double observing time. This means that for and observing time of 45 minutes the sensitivity would be only half as good. Which means fluxes of 2mJy should be detectable at 20μm. With the current fluxes this makes no difference.

Chapter 5

Discussion

In this thesis I analyzed a small part of the chemical network in ProDiMo, specifically the chemistry involving sulphur. In protoplanetary discs sulphur is observed to be depleted by roughly 2 orders of magnitude with respect to the cosmic abundance. JWST could help unraveling this mystery by providing information on the molecular composition of PPDs through the observation of ro-vibrational lines. One theory for the missing sulphur is that it is locked in non observable species. A possible candidate for those species are sulphur allotropes. Based on this I added the sulphur allotropes S_2-S_8 with their gas phase and surface chemistry to ProDiMo.

Kama et al. (2019) identified 89 $\pm$8% of the total sulphur abundance to be in refractory form in the innermost regions of a protoplanetary disc. In the vertical cuts shown in figure 4.1 sulphur allotropes have formed at 5 and 10 AU. If the formation of these sulphur allotropes is fast they could be transported with the dust to the midplane causing sulphur to be depleted. With this process it could be possible for huge amounts of sulphur to get locked in sulphur allotropes. With the stability allotropes bring locking 89% of sulphur might be possible. Kama et al. (2019) concluded that sulphide minerals were favored over sulphur allotropes because sulphide minerals are more refractory. Future work should analyze the formation of sulphide minerals and include depletion processes in inner disc regions. This could help to reproduce observations.

A problem I found and did not manage to resolve is that water flux for low C/O ratio models drops about 1 order of magnitude by including surface chemistry. All of the molecular line fluxes drop by including surface chemistry, however water seems to be the most affected. The actual abundance of H_2O in the models including surface chemistry is very similar in the inner disc compared to gas phase chemistry models. This is problematic because it is very likely that the spectral lines for water fluxes are lower than they should be. Which makes it difficult to predict if a line will be observable.

The SO and SO_2 abundance are very dependent on the C/O ratio. If this ratio exceeds 1, there are almost no sulphur oxygen species left in the gas phase chemistry. This scenario is quite extreme as more than half of the oxygen needs to be removed from the gas while carbon should remain. Two very stable ices that form within the inner disk are H_2O and CO_2, which both take more oxygen than carbon. If oxygen bearing ices form early on in the disk and the grains/pebbles settle to the midplane beyond the ice line. This causes the oxygen to be trapped inside this region. This process can remove oxygen from the gas phase leading to an increase in the C/O ratio. In figure 5.1 a vertical cut illustrating all sulphur species for a model with C/O

= 1.3 is shown.

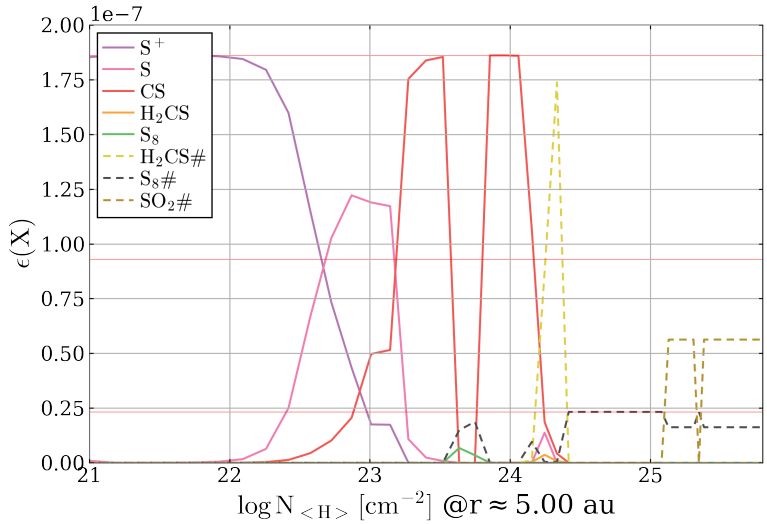

FIGURE 5.1: Vertical cuts of species abundance versus total hydrogen column density at radius 5 AU of disc model 37 with C/O = 1.3 (from table 4.1). The horizontal red lines indicate 1, 1/2 and 1/8 times the elemental sulphur abundance

The warm molecular layer around a column density of log$N_{<H>}$ = 23.5 cm^{-2} shows gas phase S_8 and S_8#. However, with oxygen depleted the only species that can react with S_8 are other sulphur allotropes. This means in order to destroy the sulphur allotropes in this regions, they need to react with themselves until S or S_2. This could be an artifact of still having too few destructive reactions. It would be interesting to know which mechanisms can make these species less stable.

C_2S lines have already been observed in protoplanetary discs (Le Gal et al., 2021). C_2S as species is not yet in the standard chemical network for ProDiMo. Furthermore they estimate that a large part of the sulphur reservoir in the outer disc could be in S-organic species ($C_xH_yS_z$). This estimate is based on a measured ratio for N(H_2CS)/N(CS) of ≈ 2/3 (Le Gal et al., 2021). S-organic species are also very limited in the model. The large DIANA network has in the gas phase the S-organic species; HCS, HCS^+, H_2CS, H_2CS^+ and H_3CS^+. It could interesting to add some extra S-organic species if there are reactions with rate coefficients available. C_2S has several reactions in the UMIST database and has been included in other models aside ProDiMo. The observation of C_2S is also interesting from the C/O ratio perspective. If C_2S is observed and SO_2 not, this could indicate an oxygen poor composition and hint at processes removing oxygen from the gas chemistry.

There are many sulphur species and reactions still available to be added to the chemical network of ProDiMo. For future research, Druard and Wakelam (2012) have information on H_2S_n and C_2S. Vidal et al. (2017) have information on H_2S_n, CS_2 , C_2S and C_3S. Semenov et al. (2018) stated that at low temperatures the gaseous HS is formed by $S + OH \rightarrow SO + H$ with a constant(b=c=0) reaction rate coefficient of $k = a =$ 0.66e-10 cm^3 s^{-1}. This reaction is neither in UMIST nor in KIDA.

If the water fluxes for the analyzed models including surface chemistry have not been depleted by more than a factor of 3 with respect to the models without surface

chemistry, detecting SO_2 should be possible for low C/O (< 0.7) ratios with JWST. If a system with C/O $\geq$ 1.1 is observed this will be very recognizable by a prominent C_2H_2 peak in the spectra around 14 μm. Figure 5.2 shows several fluxes for the model including surface chemistry with C/O = 1.1. Observing C_2H_2 or HCN is an indication that the C/O ratio is larger than 1.

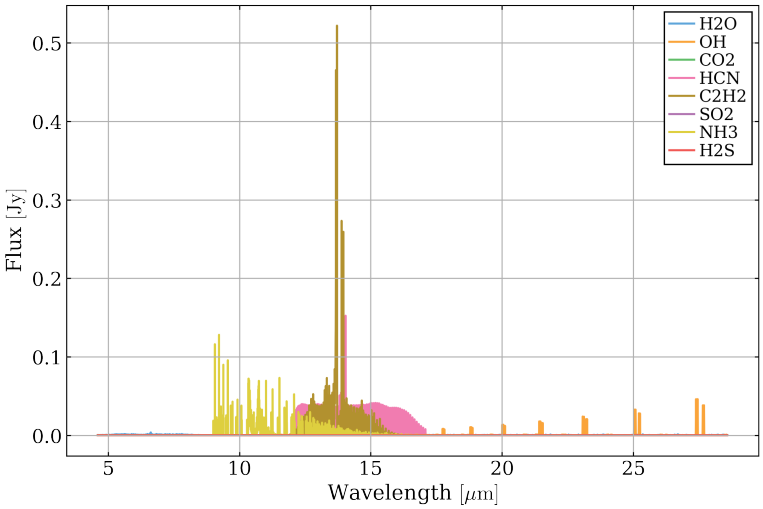

FIGURE 5.2: Spectra of several species for model 36 (surface chemistry and allotropes) from table 4.1 with C/O=1.1

H_2S is completely obscured, the fluxes I see are very faint. Might be good to see if the formation of H_2S is lacking or if the destruction is too simple. H_2S has been observed so having no abundances at all feels wrong.

Chapter 6

Conclusion

The aim of this thesis was to investigate in what form sulphur is present in the inner 10 AU of a protoplanetary disc and make spectral predictions of SO_2 to determine if this can be observed with JWST.

For the standard large DIANA chemical network with a standard TTauri disc the gaseous sulphur species in the warm molecular layer of the inner 10 AU of PPDs are in the form of S, SO and SO_2. After modifying this network by turning on surface chemistry and adding sulphur allotropes S_2 to S_8, the SO and SO_2 formation increased at radii of 5 and 10 AU for column densities of $\log N_H$ = 23 cm^{-2}. The increase in SO chemistry is due to the added reactions for sulphur allotropes. Sulphur allotropes can only react with themselves and with O to form SO. Bases on this analysis the sulphur chemistry in the warm molecular layer of the inner 10 AU was determined to be primarily oxygen-sulphur based chemistry .

Having SO and SO_2 in the gas phase makes them interesting to observe. Specifically SO_2, because of the many rovibrational lines in the wavelength range of MIRI. The visibility of SO_2 with JWST depends on how strong the water fluxes get depleted in ProDiMo when turning on surface chemistry. Based of the spectral fluxes plotted and the sensitivity of MIRI SO_2 can be observed in the ro-vibrational scissoring band (19.3 μm) in the inner 10 AU for a disc with a low C/O ratio (C/O < 0.7). Estimating that this ratio should be at least C/O $<$ 0.7. For systems having high C/O ratios (C/O > 0.7) the SO_2 fluxes drop by many orders of magnitude and will not be observable.

Acknowledgements

I would like to express the deepest appreciation to prof. dr. I.E.E. Inga Kamp, she was there for me the entire research. The pandemic hit hard and with all the regulations our weekly online meetings really helped keep me focused. Even though she had a very busy schedule, I never had to wait long for answers. The discussions, ideas, feedback and meetings were really instructive.

I'd also like to thank Romane Le Gal and David Navarro Almaida for sharing output from the three-phase model NAUTILUS and taking the time to discuss the discrepancies between both models.

Special thanks to prof. dr.Rens Waters with who I have had the pleasure discussing about sulphur.

I also had great pleasure of working with with the ISM group, presenting bits of research to discuss about really helps a project.

I am also grateful to prof. dr. Karina Caputi for being the second reader of this thesis.

Bibliography

Asplund, Martin et al. (Sept. 2009). "The Chemical Composition of the Sun". In: ARA&A 47.1, pp. 481–522. DOI: 10.1146/annurev.astro.46.060407.145222. arXiv: 0909.0948 [astro-ph.SR].

Bast, J. E. et al. (Mar. 2013). "Exploring organic chemistry in planet-forming zones". In: A&A 551, A118, A118. DOI: 10.1051/0004-6361/201219908. arXiv: 1212.3297 [astro-ph.SR].

Booth, Alice S. et al. (July 2021). "A major asymmetric ice trap in a planet-forming disk. II. Prominent SO and SO_2 pointing to C/O < 1". In: A&A 651, L6, p. L6. DOI: 10.1051/0004-6361/202141057. arXiv: 2104.08908 [astro-ph.EP].

Calmonte, U. et al. (Nov. 2016). "Sulphur-bearing species in the coma of comet 67P/Churyumov-Gerasimenko". In: MNRAS 462, S253–S273. DOI: 10.1093/mnras/stw2601.

Dionatos, Odysseas (Sept. 2015). "Gas line observations of disks". In: *European Physical Journal Web of Conferences*. Vol. 102. European Physical Journal Web of Conferences, p. 00008. DOI: 10.1051/epjconf/201510200008.

Dominik, Carsten (Sept. 2015). "Disk formation and structure". In: *European Physical Journal Web of Conferences*. Vol. 102. European Physical Journal Web of Conferences, p. 00002. DOI: 10.1051/epjconf/201510200002.

Druard, C. and V. Wakelam (2012). "Polysulphanes on interstellar grains as a possible reservoir of interstellar sulphur". In: *Monthly Notices of the Royal Astronomical Society* 426.1, 354–359. ISSN: 0035-8711. DOI: 10.1111/j.1365-2966.2012.21712.x. URL: http://dx.doi.org/10.1111/j.1365-2966.2012.21712.x.

Dubrulle, B., G. Morfill, and M. Sterzik (Apr. 1995). "The dust subdisk in the protoplanetary nebula." In: Icarus 114.2, pp. 237–246. DOI: 10.1006/icar.1995.1058.

Evans, Neal et al. (Jan. 2009). "The Diskionary: A Glossary of Terms Commonly Used for Disks and Related Objects, First Edition". In: *arXiv e-prints*, arXiv:0901.1691, arXiv:0901.1691. arXiv: 0901.1691 [astro-ph.SR].

Glasse, Alistair et al. (July 2015). "The Mid-Infrared Instrument for the James Webb Space Telescope, IX: Predicted Sensitivity". In: PASP 127.953, p. 686. DOI: 10.1086/682259. arXiv: 1508.02427 [astro-ph.IM].

Goicoechea, J. R. et al. (Sept. 2006). "Low sulfur depletion in the Horsehead PDR". In: A&A 456.2, pp. 565–580. DOI: 10.1051/0004-6361:20065260. arXiv: astro-ph/0605716 [astro-ph].

Gupta, Mukund, John Marshall, and David Ferreira (June 2019). "Triggering Global Climate Transitions through Volcanic Eruptions". In: *Journal of Climate* 32.12, pp. 3727–3742. DOI: 10.1175/JCLI-D-18-0883.1.

Henning, Thomas and Dmitry Semenov (Dec. 2013). "Chemistry in Protoplanetary Disks". In: *Chemical Reviews* 113.12, pp. 9016–9042. DOI: 10.1021/cr400128p. arXiv: 1310.3151 [astro-ph.GA].

Hobbs, Richard et al. (2021). *Sulfur Chemistry in the Atmospheres of Warm and Hot Jupiters*. arXiv: 2101.08327 [astro-ph.EP].

Kama, Mihkel et al. (Nov. 2019). "Abundant Refractory Sulfur in Protoplanetary Disks". In: ApJ 885.2, 114, p. 114. DOI: 10.3847/1538-4357/ab45f8. arXiv: 1908.05169 [astro-ph.EP].

Kamp, I. et al. (Jan. 2010). "Radiation thermo-chemical models of protoplanetary disks. II. Line diagnostics". In: A&A 510, A18, A18. DOI: 10.1051/0004-6361/200913076. arXiv: 0911.1949 [astro-ph.SR].

Kamp, I. et al. (Nov. 2017). "Consistent dust and gas models for protoplanetary disks. II. Chemical networks and rates". In: A&A 607, A41, A41. DOI: 10.1051/0004-6361/201730388. arXiv: 1707.07281 [astro-ph.SR].

Kamp, Inga (Jan. 2015). "Line radiative transfer and statistical equilibrium". In: *EPJ Web of Conferences* 102, p. 00010. DOI: 10.1051/epjconf/201510200010.

Le Gal, Romane et al. (May 2019). "Sulfur Chemistry in Protoplanetary Disks: CS and H 2 CS". In: *The Astrophysical Journal* 876, p. 72. DOI: 10.3847/1538-4357/ab1416.

Le Gal, Romane et al. (Nov. 2021). "Molecules with ALMA at Planet-forming Scales (MAPS). XII. Inferring the C/O and S/H Ratios in Protoplanetary Disks with Sulfur Molecules". In: ApJS 257.1, 12, p. 12. DOI: 10.3847/1538-4365/ac2583. arXiv: 2109.06286 [astro-ph.GA].

Macdonald, F. A. and R. Wordsworth (Feb. 2017). "Initiation of Snowball Earth with volcanic sulfur aerosol emissions". In: Geophys. Res. Lett. 44.4, pp. 1938–1946. DOI: 10.1002/2016GL072335.

Maciel, W. J. (2013). *Astrophysics of the interstellar medium*. Springer.

McElroy, D. et al. (2013). "The UMIST database for astrochemistry 2012". In: *Astronomy & Astrophysics* 550, A36. ISSN: 1432-0746. DOI: 10.1051/0004-6361/201220465. URL: http://dx.doi.org/10.1051/0004-6361/201220465.

Moses, Julianne I., Mikhail Yu. Zolotov, and Bruce Fegley (Mar. 2002). "Photochemistry of a Volcanically Driven Atmosphere on Io: Sulfur and Oxygen Species from a Pele-Type Eruption". In: Icarus 156.1, pp. 76–106. DOI: 10.1006/icar.2001.6758.

Oppenheimer, M. and A. Dalgarno (Jan. 1974). "The Chemistry of Sulfur in Interstellar Clouds". In: ApJ 187, pp. 231–236. DOI: 10.1086/152618.

Rab, Ch. et al. (Jan. 2018). "X-ray radiative transfer in protoplanetary disks. The role of dust and X-ray background fields". In: A&A 609, A91, A91. DOI: 10.1051/0004-6361/201731443. arXiv: 1711.07249 [astro-ph.SR].

Rab, Christian (2017). "Modelling of energetic processes in the circumstellar environment of young solar-like stars." In: DOI: 10.25365/thesis.50311.

Rieke, G. H. et al. (July 2015). "The Mid-Infrared Instrument for the James Webb Space Telescope, I: Introduction". In: PASP 127.953, p. 584. DOI: 10.1086/682252. arXiv: 1508.02294 [astro-ph.IM].

Rothman, L.S. et al. (2013). "The HITRAN2012 molecular spectroscopic database". In: *Journal of Quantitative Spectroscopy and Radiative Transfer* 130. HITRAN2012 special issue, pp. 4–50. ISSN: 0022-4073. DOI: https://doi.org/10.1016/j.jqsrt.2013.07.002. URL: https://www.sciencedirect.com/science/article/pii/S0022407313002859.

Ruaud, Maxime, Valentine Wakelam, and Franck Hersant (Apr. 2016). "Gas and grain chemical composition in cold cores as predicted by the Nautilus three-phase model". In: *Monthly Notices of the Royal Astronomical Society* 459.4, pp. 3756–3767. ISSN: 0035-8711. DOI: 10.1093/mnras/stw887. eprint: https://academic.oup.com/mnras/article-pdf/459/4/3756/8191920/stw887.pdf. URL: https://doi.org/10.1093/mnras/stw887.

Rybicki, George B and Alan P Lightman (1985). *Radiative Processes in Astrophysics*. New York, NY: Wiley. DOI: 10.1002/9783527618170. URL: https://cds.cern.ch/record/847173.

Semenov, D. et al. (Sept. 2018). "Chemistry in disks. XI. Sulfur-bearing species as tracers of protoplanetary disk physics and chemistry: the DM Tau case". In: A&A 617, A28, A28. DOI: 10.1051/0004-6361/201832980. arXiv: 1806.07707 [astro-ph.GA].

Shaw, Andrew M. (2007). *Astrochemistry: From astronomy to astrobiology*. Wiley.

Sternberg, A. and A. Dalgarno (Aug. 1995). "Chemistry in Dense Photon-dominated Regions". In: ApJS 99, p. 565. DOI: 10.1086/192198.

Theilig, E. et al. (1982). *A Primer on Sulfur for the Planetary Geologist*. NASA contractor report. National Aeronautics, Space Administration, Scientific, and Technical Information Branch. URL: https://books.google.nl/books?id=NJIzAQAAIAAJ.

Thi, W. F., P. Woitke, and I. Kamp (Apr. 2011). "Radiation thermo-chemical models of protoplanetary discs - III. Impact of inner rims on spectral energy distributions". In: MNRAS 412.2, pp. 711–726. DOI: 10.1111/j.1365-2966.2010.17741.x. arXiv: 1009.4374 [astro-ph.GA].

Thi, W. F. et al. (Dec. 2018). "Warm dust surface chemistry. H2 and HD formation". In: *arXiv e-prints*, arXiv:1812.06730, arXiv:1812.06730. arXiv: 1812.06730 [astro-ph.GA].

Vidal, Thomas H. G. et al. (July 2017). "On the reservoir of sulphur in dark clouds: chemistry and elemental abundance reconciled". In: MNRAS 469.1, pp. 435–447. DOI: 10.1093/mnras/stx828. arXiv: 1704.01404 [astro-ph.GA].

Waters, L. B. F. M. (Sept. 2015). "Dust in protoplanetary disks: observations". In: *European Physical Journal Web of Conferences*. Vol. 102. European Physical Journal Web of Conferences, p. 00003. DOI: 10.1051/epjconf/201510200003.

Wells, Martyn et al. (2015). "The Mid-Infrared Instrument for theiJames Webb Space Telescope/i, VI: The Medium Resolution Spectrometer". In: *Publications of the Astronomical Society of the Pacific* 127.953, pp. 646–664. DOI: 10.1086/682281. URL: https://doi.org/10.1086/682281.

Williams, Jonathan P. and Lucas A. Cieza (2011). "Protoplanetary Disks and Their Evolution". In: *Annual Review of Astronomy and Astrophysics* 49.1, 67–117. ISSN: 1545-4282. DOI: 10.1146/annurev-astro-081710-102548. URL: http://dx.doi.org/10.1146/annurev-astro-081710-102548.

Woitke, P. et al. (Feb. 2016). "Consistent dust and gas models for protoplanetary disks. I. Disk shape, dust settling, opacities, and PAHs". In: A&A 586, A103, A103. DOI: 10.1051/0004-6361/201526538. arXiv: 1511.03431 [astro-ph.EP].

Woitke, P. et al. (Oct. 2018). "Modelling mid-infrared molecular emission lines from T Tauri stars". In: A&A 618, A57, A57. DOI: 10.1051/0004-6361/201731460. arXiv: 1807.05784 [astro-ph.SR].

Woitke, Peter (Sept. 2015a). "Heating and cooling processes in disks". In: *European Physical Journal Web of Conferences*. Vol. 102. European Physical Journal Web of Conferences, p. 00011. DOI: 10.1051/epjconf/201510200011.

— (Sept. 2015b). "Modelling and interpretation of SEDs". In: *European Physical Journal Web of Conferences*. Vol. 102. European Physical Journal Web of Conferences, p. 00007. DOI: 10.1051/epjconf/201510200007.

Woitke, P., Kamp, I., and Thi, W.-F. (2009). "Radiation thermo-chemical models of protoplanetary disks - I. Hydrostatic disk structure and inner rim". In: *A&A* 501.1, pp. 383–406. DOI: 10.1051/0004-6361/200911821. URL: https://doi.org/10.1051/0004-6361/200911821.

Appendix A

Appendix A

The following tables include all reactions concerning sulphur allotropes that I added to the chemical network.

	reaction		a	b	c
1	S + S + M	→ S2	3.95E-33	0.00E+00	0.00E+00
2	S + S2 + M	→ S3	1.11E-30	-2.00E+00	0.00E+00
3	S + S3 + M	→ S4	1.11E-30	-2.00E+00	0.00E+00
4	S + S4 + M	→ S5	1.11E-30	-2.00E+00	0.00E+00
5	S + S5 + M	→ S6	1.11E-30	-2.00E+00	0.00E+00
6	S + S6 + M	→ S7	1.11E-30	-2.00E+00	0.00E+00
7	S + S7 + M	→ S8	1.11E-30	-2.00E+00	0.00E+00
8	S2 + S2 + M	→ S4	2.20E-29	0.00E+00	0.00E+00
9	S2 + S3 + M	→ S5	1.11E-30	-2.00E+00	0.00E+00
10	S2 + S4 + M	→ S6	1.11E-30	-2.00E+00	0.00E+00
11	S2 + S5 + M	→ S7	1.11E-30	-2.00E+00	0.00E+00
12	S2 + S6 + M	→ S8	1.11E-30	-2.00E+00	0.00E+00
13	S3 + S3 + M	→ S6	1.00E-30	0.00E+00	0.00E+00
14	S3 + S4 + M	→ S7	1.11E-30	-2.00E+00	0.00E+00
15	S3 + S5 + M	→ S8	1.11E-30	-2.00E+00	0.00E+00
16	S4 + S4 + M	→ S8	1.00E-30	0.00E+00	0.00E+00
17	S + S3	→ S2 + S2	8.00E-11	0.00E+00	0.00E+00
18	S + S4	→ S2 + S3	8.00E-11	0.00E+00	0.00E+00
19	S + S5	→ S2 + S4	5.00E-11	0.00E+00	2.00E+02
20	S + S6	→ S2 + S5	5.00E-11	0.00E+00	3.00E+02
21	S + S7	→ S2 + S6	4.00E-11	0.00E+00	2.00E+02
22	S + S8	→ S2 + S7	4.00E-11	0.00E+00	4.00E+02
23	S + S5	→ S3 + S3	3.00E-11	0.00E+00	2.00E+02
24	S + S6	→ S3 + S4	3.00E-11	0.00E+00	3.00E+02
25	S + S7	→ S3 + S5	2.00E-11	0.00E+00	2.00E+02
26	S + S8	→ S3 + S6	2.00E-11	0.00E+00	4.00E+02
27	S + S7	→ S4 + S4	2.00E-11	0.00E+00	2.00E+02
28	S + S8	→ S4 + S5	2.00E-11	0.00E+00	4.00E+02
29	S2 + S8	→ S5 + S5	1.00E-11	0.00E+00	1.40E+03
30	S3 + S5	→ S2 + S6	4.00E-11	0.00E+00	2.00E+02
31	S3 + S7	→ S2 + S8	3.00E-11	0.00E+00	2.00E+02
32	S3 + S7	→ S4 + S6	1.00E-11	0.00E+00	2.00E+02
33	S3 + S4	→ S2 + S5	4.00E-11	0.00E+00	2.00E+02
34	S3 + S6	→ S2 + S7	4.00E-12	0.00E+00	3.00E+02
35	S3 + S7	→ S5 + S5	1.00E-11	0.00E+00	2.00E+02
36	S4 + S5	→ S2 + S7	2.00E-12	0.00E+00	2.00E+02

37	S4 + S6	→ S2 + S8	2.00E-12	0.00E+00	3.00E+02
38	S4 + S5	→ S3 + S6	2.00E-12	0.00E+00	2.00E+02
39	S4 + S7	→ S3 + S8	5.00E-12	0.00E+00	2.00E+02
40	S4 + S6	→ S5 + S5	2.00E-12	0.00E+00	3.00E+02
41	S4 + S7	→ S5 + S6	5.00E-12	0.00E+00	2.00E+02
42	O + S3	→ S2 + SO	8.00E-11	0.00E+00	0.00E+00
43	O + S4	→ S3 + SO	8.00E-11	0.00E+00	0.00E+00
44	O + S5	→ S4 + SO	8.00E-11	0.00E+00	2.00E+02
45	O + S6	→ S5 + SO	8.00E-11	0.00E+00	3.00E+02
46	O + S7	→ S6 + SO	8.00E-11	0.00E+00	2.00E+02
47	O + S8	→ S7 + SO	8.00E-11	0.00E+00	4.00E+02

TABLE A.1: Gas phase reactions included ProDiMo from (Hobbs et al., 2021)

	reaction		a	b	c
1	S# + S#	→ S2#	1.00E+00	0.00E+00	0.00E+00
2	S2# + S#	→ S3#	1.00E+00	0.00E+00	0.00E+00
3	S2# + S2#	→ S4#	1.00E+00	0.00E+00	0.00E+00
4	S3# + S#	→ S4#	1.00E+00	0.00E+00	0.00E+00
5	S4# + S#	→ S5#	1.00E+00	0.00E+00	0.00E+00
6	S3# + S2#	→ S5#	1.00E+00	0.00E+00	0.00E+00
7	S5# + S#	→ S6#	1.00E+00	0.00E+00	0.00E+00
8	S4# + S2#	→ S6#	1.00E+00	0.00E+00	0.00E+00
9	S3# + S3#	→ S6#	1.00E+00	0.00E+00	0.00E+00
10	S6# + S#	→ S7#	1.00E+00	0.00E+00	0.00E+00
11	S5# + S2#	→ S7#	1.00E+00	0.00E+00	0.00E+00
12	S4# + S3#	→ S7#	1.00E+00	0.00E+00	0.00E+00
13	S7# + S#	→ S8#	1.00E+00	0.00E+00	0.00E+00
14	S6# + S2#	→ S8#	1.00E+00	0.00E+00	0.00E+00
15	S5# + S3#	→ S8#	1.00E+00	0.00E+00	0.00E+00
16	S4# + S4#	→ S8#	1.00E+00	0.00E+00	0.00E+00

TABLE A.2: Surface chemistry reactions included in ProDiMo added from Druard and Wakelam (2012)